



### Institutional Sign In

All



ADVANCED SEARCH

Journals & Magazines > IEEE Transactions on Systems,... > Volume: 46 Issue: 2

# Automated Opal Grading by Imaging and Statistical Learning

Publisher: IEEE

[Cite This](#)

[PDF](#)

Dadong Wang ; Leanne Bischof ; Ryan Lagerstrom ; Volker Hilsenstein ; Angus Hornabrook ; Graham Hornabrook [All Authors](#)

10  
Cites in  
Papers

2141  
Full  
Text Views



## Alerts

[Manage Content Alerts](#)  
[Add to Citation Alerts](#)

[Open Access](#)

### Abstract



Downl  
PDF

PDF

Help

#### Document Sections

- I. Introduction
- II. Gemological Digital Analyzer
- III. Image Capture and Calibration
- IV. Feature Extraction
- V. Automated Opal Classification and Grading

[Show Full Outline](#)

[Authors](#)

[Figures](#)

[References](#)

[Citations](#)

[Keywords](#)

[Metrics](#)

#### Abstract:

Quantitative grading of opals is a challenging task even for skilled opal assessors. Current opal evaluation practices are highly subjective due to the complexities of op... [View more](#)

#### Metadata

##### Abstract:

Quantitative grading of opals is a challenging task even for skilled opal assessors. Current opal evaluation practices are highly subjective due to the complexities of opal assessment and the limitations of human visual observation. In this paper, we present a novel machine vision system for the automated grading of opals-the gemological digital analyzer (GDA). The grading is based on statistical machine learning with multiple characteristics extracted from opal images. The assessment workflow includes calibration, opal image capture, image analysis, and opal classification and grading. Experimental results show that the GDA-based grading is more consistent and objective compared with the manual evaluations conducted by the skilled opal assessors.

**Published in:** IEEE Transactions on Systems, Man, and Cybernetics: Systems ( Volume: 46 , Issue: 2, February 2016)

**Page(s):** 185 - 201

**DOI:** 10.1109/TSMC.2015.2427776

**Date of Publication:** 14 May 2015

**Publisher:** IEEE

#### ISSN Information:

#### Funding Agency:

## SECTION I.

# Introduction



Opal is the national gemstone of Australia, which produces 95% of the world's supply and supports a historic opal mining industry. Current precious opal assessment and evaluation practices are highly subjective and inconsistent as they are based on a combination of human observed factors, such as color, brightness, saturation, shape, pattern, cut, inclusions, play of color (POC), etc. [1]–[5]. The assessment is made using a magnification  $10\times$  loupe by holding an opal in a pair of tweezers and smoothly rolling it through all three axes (roll, pitch, and yaw) to observe light interaction with the opal, along with external and internal characteristics. The light is normally from a window falling over the observer's shoulder so that the angle of illumination and the angle of observation are the same. A unique characteristic of opal, called flash, is the display of varying bright colors. It is caused by the interaction of light with microscopic silica spheres. The size of the sphere determines the observed flash color. The flash color (hue, brightness, and saturation) and body tone of a precious opal have significant weight in the overall grade and ultimately the value of the precious opal. However, when seeking an objective assessment by a human observer, the colors, body tone, POC, and directionality appear to be the most difficult to quantify. The body tone is the background color of an opal. It refers to the relative darkness or brightness of the opal while ignoring its flash and POC. The POC is a phenomenon of the flash of a specific color changing position, or a specific region of the flash changing color, as the viewing angle is changed. The directionality is the frequency of the area of the color flash displayed from all angles. Due to the variability and complex reflectance properties of opals, experts such as experienced gemologists, consider opals to be one of the hardest gemstones to appraise. Many participants in the opal supply chain do not even have the training to assess the grade or value of opals being supplied. This has led to a lack of confidence in trading opals. The difficulty in describing a particular opal type or quality, in sufficiently concise and objective terms, complicates negotiations between buyers and sellers. This poses a challenge for suppliers to provide appropriate opals, or for the suppliers and buyers to reach agreement on the grade or value of the opals.

A comprehensive literature review reveals that there has been no automated opal grading system reported to date. A device for measuring characteristics of a gemstone was invented by Valente *et al.* [6] in 1997. This device uses a band pass filter and detector array to obtain the spectral response of a complete image. The device provides spectral photometric data for each individual pixel of the image, and utilizes multiple lighting angles to construct a composite image for gemstone grading. In the same year, Michael *et al.* [7] filed their patent, "Gemstone registration system"—a system which can be used to record and retrieve the optical images of gemstones using a 2-D charge-coupled device (CCD). In 1998, Valente *et al.* [8] demonstrated a device for measuring characteristics of a gemstone by detecting the light frequency response of said gemstone under illumination. Shannon [9] proposed a system for computerized grading of the cut of a gemstone in 1999. This system includes a gemstone model and an illumination model. In 2001, Aggarwal [10] claimed a system for generating, maintaining, and retrieving characterizing information for standardized grading of gemstones. This system gauges the spectral response of a gemstone subject to a plurality of incident light sources within an imaging apparatus. An invention was also published in 2001, which is comprised of the systems, apparatuses, and methods for measuring and analyzing gem color and approximating visual analysis methodology [11]. The three elements of this system include a daylight approximating light source, a light detector, and an optical measurement device. Sevdermish [12] published a system for digital color grading of gems in 2003. It includes a computer-based expert system and methodology for grading gems using their inherent properties of shape and color. The grading is conducted interactively on-screen by visual comparison to the image of a real-target gem, and the result, translated into alpha-numeric code, can be communicated by phone or via the Internet to any other user of the same system and database. A computerized system for teaching an untrained observer to evaluate a gemstone was published in 2005 [13]. The computer was connected to an apparatus capable of capturing an image of a gemstone. The image was processed using the computer to determine one or more

optical properties of the gemstone. Haske and Caruso [14] reported a SAS2000 spectrophotometer analysis system for diamond and gemstone evaluation and grading. The system can provide accurate colorimetry for diamond color grading. A method and associated apparatus for the standardized grading of gemstones was also patented in 2005 [15]. Gemstone qualities are analyzed by using a plurality of light sources from an imaging apparatus. Light energy data is captured in the form of pixel data sets via a CCD. A gemstone is then quantified using the pixel data sets. In 2007, Holloway [16] was granted a patent for his invention of a system and method for providing gem assessments based upon proportional parameter values relating to the proportions of a gem. A gem cut quality rating is provided. The system and method are suited for use in an online environment or may be utilized in conjunction with rough diamond analysis instruments in order to provide cutters with guidance to maximize the yield of a rough diamond. Methods and devices for assessing diamond colors were also published in 2007 [17]. With these methods and devices, the color and other quality properties of finished diamonds, cut from a given rough diamond, can be assessed by analysis of the rough diamond. In 2008, Sasian *et al.* [18] were granted a patent for their methods, apparatuses, and systems for evaluating gemstones. These methods trace rays through a computer representation of a gemstone wherein the rays enter the gemstone through the gemstone crown and allow a grade to be assigned to the gemstone. A method and system for color grading of gemstone was also patented by Liu [19]. This method and system includes a function to generate a reference color and a computer program for color grading of gemstones by matching the reference color to that of the gemstone graded. In 2010, a study was conducted into 3-D mathematical modeling to investigate the interaction of light with a fully faceted, colorless, symmetrical round-brilliant-cut diamond [20]. In 2011, Guo *et al.* [21] presented their linear discriminant model for assessing green colored gemstones, jadeite-jade, turquoise, and emerald. In 2013, an amber gemstone classification system was proposed and described in [22]. The amber data were collected by amber industry experts and divided manually into 30 classes. The authors used these data to test various classifiers such as quadratic discriminant analysis,  $K$ -nearest neighbor, radial basis function (RBF), and decision tree. The best classification result was 60.3% accuracy which was produced from a pruned decision tree classifier. Verboven and Blodgett [23] were granted a patent for their method and system for generating a clarity grading look-up table. The method and system includes the collection of actual inclusion parameter data for a plurality of gems, and a mathematical model for formulating a clarity grade and a particular inclusion parameter combination. More recently in 2014, Benjano [24] published his method and apparatus for the grading of gemstone cut. His invention includes a system for controlling the cut of a gemstone. It is composed of a gemstone scanner adapted to scan a plurality of gemstone facets using a control module coupled to the scanner. The control module can generate an actual 3-D model of the gemstone. The system is broadly related to the field of gemstone grading and but more particularly to controlling the cut of a gemstone. A computerized method and system for light performance grading of gemstones was also published by Levami and Caspi [25] in 2014. The method and system can be used to produce a single grading scale for evaluating gemstones based on predefined parameters. Each single grade in the scale is associated with unique groups of parameter value ranges in a statistically relevant sample of gemstones. Quick also published his invention of systems and methods for generating gemstone images which are coded according to angular ranges in their angular spectrum across a broad range of tilts. This allows for the scintillation of a gemstone to be demonstrated based on a singular coded image of the gemstone. Fire scintillation, flash scintillation, and other scintillation related criteria are shown as a series of static images [26].

Although there are some existing technologies for assessing diamonds and colored gemstones, none of these systems is suitable for the detection or analysis of unique opal characteristics, such as “body tone,” “POC,” and “directionality.”

In this paper, we present a machine vision system which is named the gemological digital analyzer (GDA). The GDA can be used to automatically and objectively grade opals based on their reflectance characteristics. To accurately assess an opal, it is scanned over the full range of viewing angles ( $0^\circ$ – $360^\circ$  of rotation and  $0^\circ$ – $90^\circ$  of tilt angles, giving full coverage of the opal’s face) with different lighting angles and camera exposures. In total 865 images are acquired from each opal to be assessed. These images are then quantified to extract quality features of the opal, which are used to automatically classify the opal into one of several opal classes. Based on class specific grading models, the measured opal features are employed as inputs to class-specific support vector regression (SVR) models for calculating the gem score of the opal. The gem score is a term we have defined to reflect how precious an opal is. It is an opal measure on a per carat basis, and is used as

the criterion to grade opals. We then use the gem score to produce the opal grade which is associated with the averaged value of the opal per carat.

We have developed the world's first machine vision system for the automated grading of opals. Our contributions to the technique of automatic opal grading include: 1) scientifically defined, in a quantifiable way, important features for opal grading, such as flash, body tone, directionality, and POC; 2) developed complex image analysis algorithms for extracting the opal features; 3) successfully mimicked the manual assessment process of an opal by developing the machine vision system and the imaging procedure for the opal grading; and 4) by using imaging and machine learning, incorporated into the GDA the domain knowledge of over 60 experienced opal industry experts, with cumulatively over 1000 years of opal assessment experience.

The GDA system is introduced in the next section, followed by the opal image capture and calibration in Section III. Section IV describes the opal image analysis for extracting opal features, and outlines how to accelerate the image processing. The automated opal classification and grading method is presented in Section V with detailed experimental results. This is followed by the conclusion in Section VI.

## SECTION II. Gemological Digital Analyzer

### A. GDA Architecture

The GDA is an automated device for grading opals using imaging and statistical learning. The GDA hardware is designed to mimic the human observation of an opal by rotating it under controlled lighting and capturing its images. The opal images are then analyzed by the software which takes objective and repeatable measurements of the opal's multiple characteristics such as color, brightness, body tone, etc. The measurements are piped into a database for subsequent automated opal classification and grading based on statistical machine learning (SML). The measurements and the grading results of an opal are designed to be retrieved remotely by an opal trading information system (OTIS) which can be accessed through the Internet, by authorized personnel. Fig. 1 shows the hardware of the GDA.

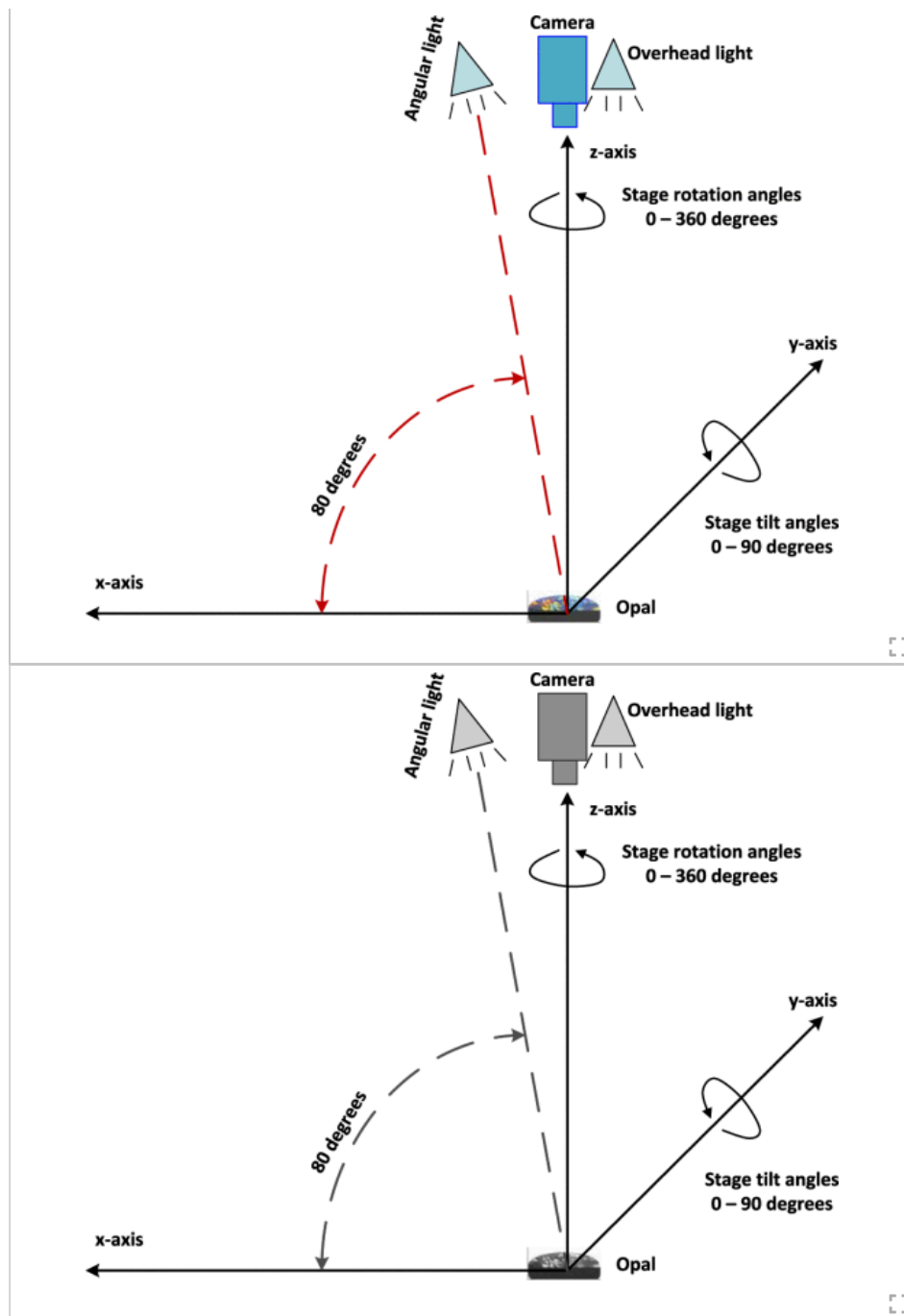




**Fig. 1.**  
Motorized rotation stage and mainframe of the GDA.

In detail, the GDA is comprised of the following components.

- 1) An image capture system including a two-axis translucent stage on which an opal can be held using suction from beneath the opal; white LED lighting mounted below the stage; a 5-megapixel camera with 10 bits digital output; one overhead and one angular halogen light mounted directly above the rotation stage with the angular light pointed at an angle of  $80^\circ$  to the stage. The overhead and angular lights are positioned close to the camera so that the illumination angle and viewing angle are nearly coincident. This is to replicate the lighting conditions used for human opal grading. The stage can rotate from  $0^\circ$  to  $360^\circ$  within the horizontal plane (about the  $z$ -axis) and tilt from  $0^\circ$  to  $90^\circ$  of elevation (about the  $y$ -axis). Fig. 2 shows the three axes, the relative position of the camera and the light sources, along with the stage rotation and tilt angles. A suction system secures the opal to the stage. The suction cup and associated tubing from the cup to the vacuum pump are translucent. The suction system, therefore, does not occlude the opal in either the forward or back lit views.
- 2) Specially developed software for automating the hardware to capture opal images, carrying out image analysis to extract opal features, and conducting opal classification and grading.
- 3) A backend database for storing and retrieving all opal information including their assessment results generated by the GDA.



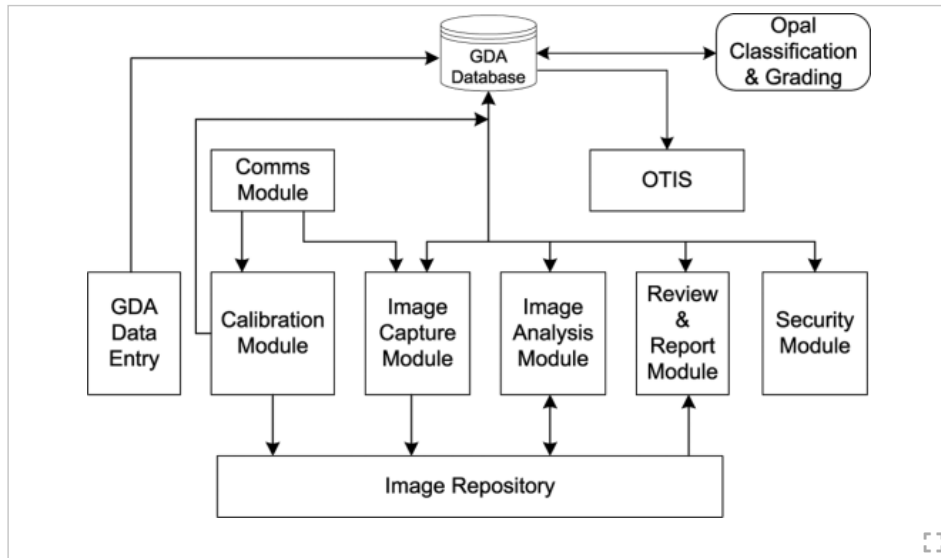
**Fig. 2.** Definition of axes, the relative position of the camera and the light sources, the stage rotation, and tilt angles.

## B. GDA Software

The GDA software analyzes the opal images to extract a summary of the flash, body tone, and other characteristics. The software uses these characteristics to automatically classify the opal into one of several opal classes and then grade the opal.

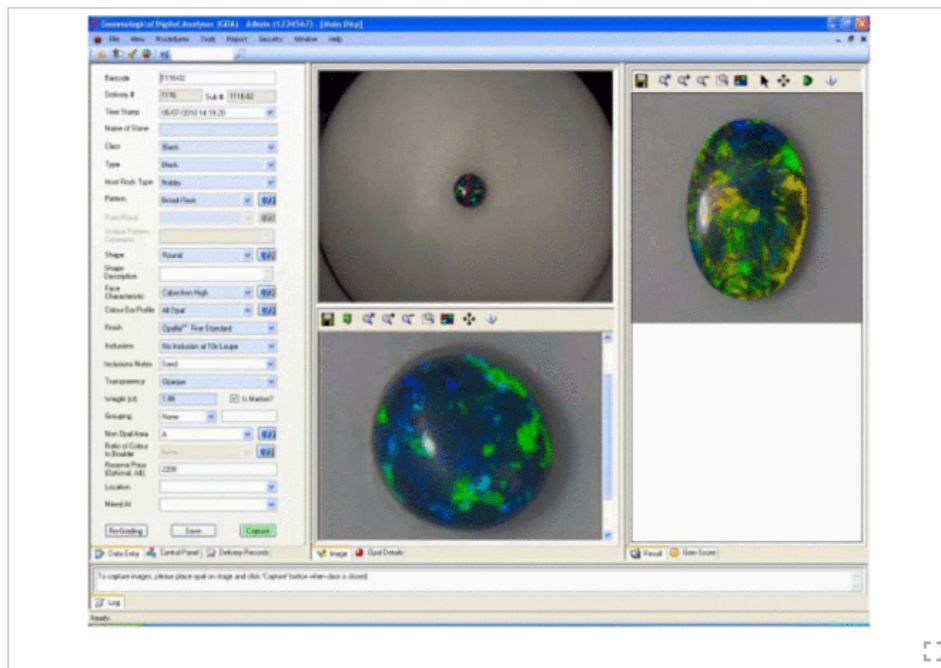
Fig. 3 illustrates the software components of the GDA software. In Fig. 3, GDA data entry provides an interface for an operator to enter opal details such as delivery number, opal shape, pattern, and class based on the operator's observation or information provided by the opal miner. These manually entered data are stored in the GDA database and are retrieved in the image capture, analysis, reporting, classification, and grading processes. The comms module is responsible for serial communications between various hardware controllers and the GDA computer. It involves driving the hardware of the GDA, such as the camera, lighting, and the rotation stage in the GDA mainframe, along with a Sartorius scale to weigh the opal. The calibration module is designed for

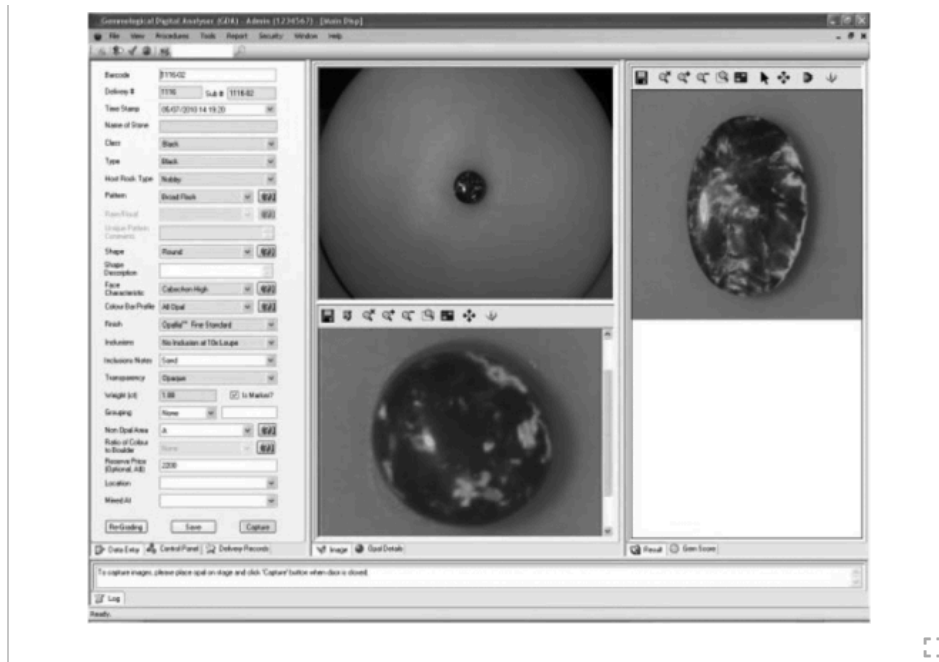
lighting correction and color calibration. The calibration records are stored in the GDA database and the images captured in the calibration process are stored in the image repository. The image capture module is for automatic opal image capture, controlling the stage rotation and tilt, switching on and off the different light sources, changing camera exposure settings, and acquiring opal images from the camera. The captured images are stored in the image repository. The image analysis module measures color feature characteristics of raw opal images which are stored in the image repository. The quantified characteristics are stored in the GDA database and the processed result images are stored in the image repository. The review and report module provides interfaces for GDA users to view GDA calibration reports, system logs and operation reports. The security module is designed for system administration such as setting up and updating user login and privilege details. The opal classification and grading module is designed to automatically identify the class of an opal and then use a class specific model to grade the opal. The grading results are stored in the GDA database.



**Fig. 3.** Software component diagram of the GDA.

The OTIS is not part of the GDA, but an external trading system which remotely accesses the GDA database and presents quantification and grading information to the OTIS administrators or potential opal buyers. Fig. 4 shows the graphical user interface (GUI) of the GDA software.





**Fig. 4.**  
GUI of the GDA software.

## SECTION III. Image Capture and Calibration

The measurements produced by the GDA must be repeatable over time. However, there are components of the GDA that do vary over time. In particular, the light source intensity can deteriorate, the color sensors in the camera can change and the color reference (Macbeth card) used for the calibration may fade over the time. To correct for these variations, calibration of the GDA needs to be carried out on a daily basis before any opal images are captured.

The calibration involves a number of steps that include the following.

- 1) Lighting correction with white and gray cards.
- 2) Spatial calibration with graph cards.
- 3) Color calibration with a Macbeth color card.
- 4) Standard benchmark stone calibration check.

The calibration process produces a number of images, referred to as the calibration set. From the calibration set a number of measurements and correcting transformations are computed. Every opal that is scanned by the GDA is linked to its appropriate calibration set. When an opal is analyzed, its data are standardized against its calibration set, allowing the GDA to reliably compare measurements over time [27], [28].

### A. Image Calibration

#### 1) Extended Exposure:

The reflectance of opals covers a very wide dynamic range, from very dark areas of body tone to flash regions that are typically orders of magnitude brighter. This range of reflectance exceeds the dynamic range that a standard camera can capture in a single image. To capture the full dynamic range encountered in opals without losing information due to over- or under-exposure, a pair of images is captured at different exposure times. The chosen camera has a 10-bit dynamic range for each red (R), green (G), and blue (B) channel image giving pixel gray values in the range of 0–

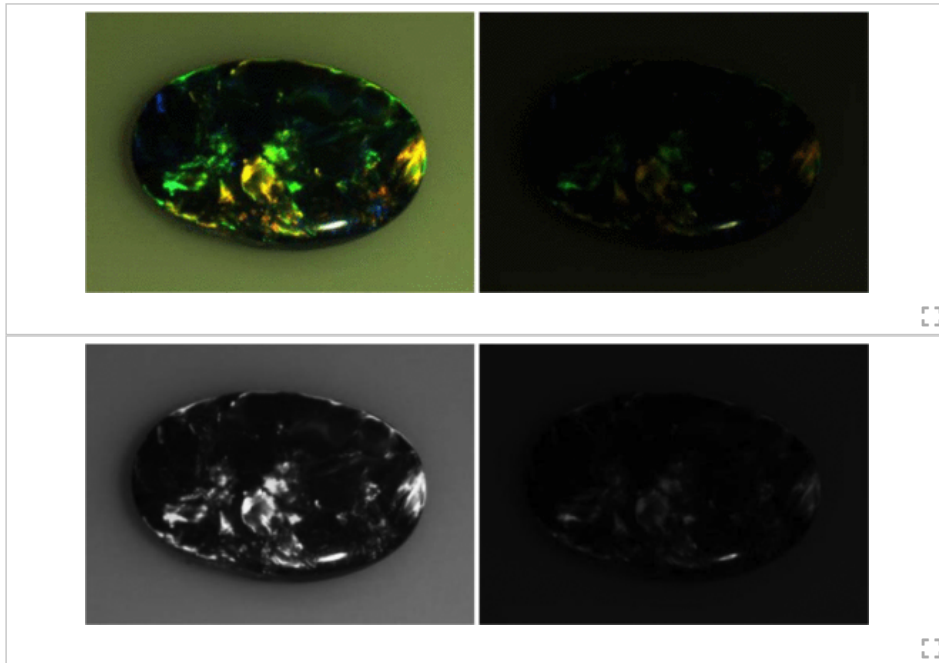


1023. Images  $I_{\text{short}}$  and  $I_{\text{long}}$  are captured at two exposures, 2 and 32 ms, respectively, and combined to give an image of extended dynamic range,  $I_{\text{ext}}$ , as shown in (1). This gives a gray value range of 0–16 284. We experimentally established that no opals have a gray value of over 10 000

$$I_{\text{ext}} = \begin{cases} I_{\text{long}} & \text{if } I_{\text{long}} < \text{threshold} \\ I_{\text{short}} \cdot \text{scaling} & \text{if } I_{\text{long}} \geq \text{threshold} \end{cases} \quad (1)$$

[View Source](#)

where threshold is 900, and scaling is given by the ratio of the means of  $I_{\text{long}}/I_{\text{short}}$  for a standard Kodak white card. Fig. 5 shows a comparison of images captured with long and extended exposures of the same opal.



**Fig. 5.** Comparison of the images captured with the long exposure (left) and the extended exposure (right).

### 2) Lighting Correction:

With a single light source, the lighting is often not uniform across the field of view of the camera. It will tend to be brighter in the center of the lighting field. To correct for these lighting nonuniformities, two lighting field images are acquired,  $I_{\text{white}}$  and  $I_{\text{gray}}$ , of standard Kodak white and gray cards, respectively. The Kodak white card has 90% reflectance across the visible spectrum and the Kodak gray card has 18% reflectance. Assuming the CCD sensors in the camera are linear, these lighting field images can be used to correct the extended range image  $I_{\text{ext}}$  consisting of the channels  $R_{\text{ext}}$ ,  $G_{\text{ext}}$ , and  $B_{\text{ext}}$ . The lighting corrected image  $I_{\text{cor}}$  is derived

$$L_{\text{max}} = \max(\text{mean}(R_{\text{ext}}), \text{mean}(G_{\text{ext}}), \text{mean}(B_{\text{ext}}))$$

$$I_{\text{cor}} = (I_{\text{ext}} - I_{\text{gray}}) L_{\text{max}} \frac{90-18}{90} + L_{\text{max}} 18/90. \quad (2)$$

[View Source](#)

### 3) Color Calibration:

Because the CCD sensors in color cameras can have different sensitivities and because the spectral characteristics of the light source can vary with time, the lighting corrected image,  $I_{\text{cor}}$  is specific to the hardware setup. In other words, it is a device-dependent, relative measure of color. We need to

carry out color calibration to convert the device-specific RGB image captured by the GDA to a device-independent, absolute measure of color.

a) Device-Specific RGB to Device-Independent XYZ:

In order to convert from device-specific RGB values to device-independent XYZ values, as defined by the International Commission on Illumination [29], we need a calibrated color checker card, such as a Macbeth card, which has several color swatches of known device-independent XYZ values. By capturing an image of this card and extracting the mean RGB values for each color swatch, the transformation matrix,  $RGB2XYZ$ , can be determined by linear regression between the measured RGB values and the supplied XYZ values. Thus the RGB values in the  $I_{cor}$  image can be converted to XYZ values in the  $I_{XYZ}$  image using this matrix.

b) Device-Independent XYZ to Device-Independent sRGB:

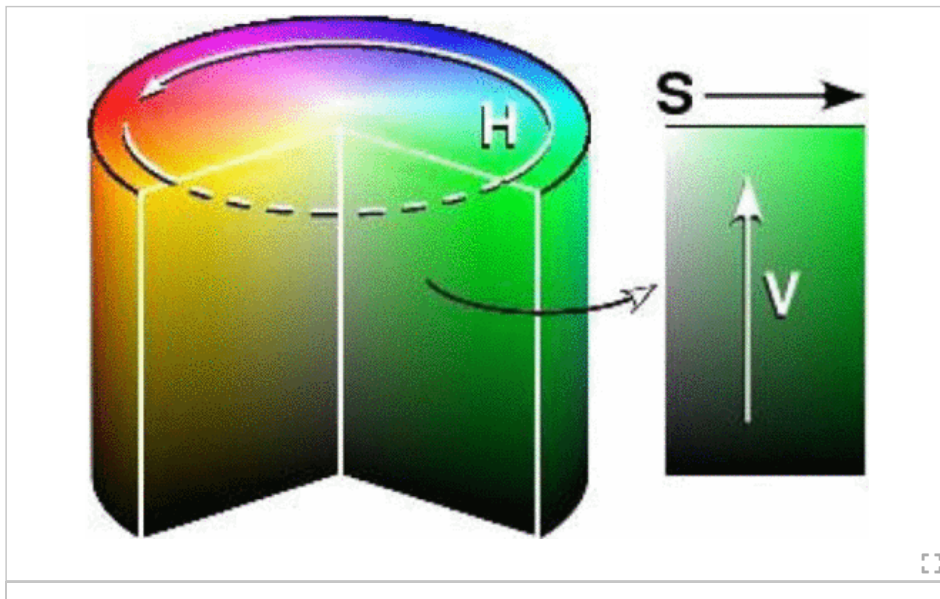
Although the device-independent XYZ measure of color is an internationally recognized standard for color representation, it is linear (unlike the human visual system) and not easily understood by nonexperts. So, we have chosen to convert the XYZ measure to a standard RGB representation, called sRGB [30]. The D65 illuminant of this standard is designed to match noon daylight which is typical of home and office viewing conditions. The nonlinear transfer function (gamma curve) closely matches that of the human visual system. If sRGB images of opals are viewed on sRGB calibrated monitors they will closely match the actual opal appearance if viewed under natural daylight (D65 lighting conditions). We convert the  $I_{XYZ}$  image to the sRGB calibrated image,  $I_{sRGB}$ , using the standard transformation matrix,  $XYZ2sRGB$

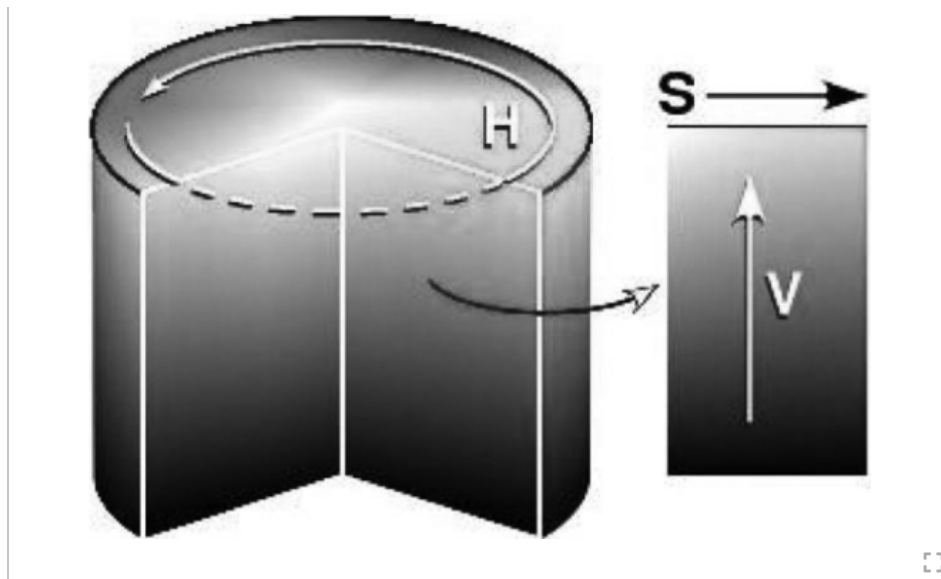
$$\begin{pmatrix} R \\ G \\ B \end{pmatrix} = \begin{pmatrix} 3.240479 & -1.537150 & -0.498535 \\ -0.969256 & 1.875992 & 0.041556 \\ 0.055648 & -0.204043 & 1.057311 \end{pmatrix} \begin{pmatrix} X \\ Y \\ Z \end{pmatrix}. \quad (3)$$

[View Source](#)

4) Color Transformation From sRGB to sHSB:

The RGB representation of color is commonly used in image capture and display devices, but it is not designed for describing human perception of color. For this, we transform the sRGB image to an alternative representation of color called HSB (or HSV). HSB stands for hue, saturation, and brightness (also known as value). Hue is a measure of the dominant wavelength of a color and is given as an angle between  $0^\circ$  and  $360^\circ$ . Saturation is a measure of the purity of color or the amount of white added. A pure color will have 100% saturation. For decreasing values of saturation, the pure color is increasingly diluted with white. The brightness (or value) is a measure of the intensity of the color. The brightest color will have 100% brightness. Fig. 6 shows the HSB representation of color. For decreasing values of brightness, the pure color is increasingly diluted with black. In our extended exposure images, our brightest color  $B_{max}$  (100%) has been scaled to 3000.





**Fig. 6.**  
HSB (value) representation of color.

Because HSB is a transformation of the RGB values in an image, it is defined relative to the standards of the RGB values. Transforming sRGB values will give standardized “sHSB” values, relative to the D65 white point. Applying the following RGB2HSB transformation to the  $I_{sRGB}$  image, gives the image  $I_{sHSB}$  :

$$H = \begin{cases} 0 & \text{if } \max = \min \\ \frac{60^\circ (g - b)}{\max - \min} + 0^\circ & \text{if } \max = r \geq b \\ \frac{60^\circ (g - b)}{\max - \min} + 360^\circ & \text{if } \max = r < b \\ \frac{60^\circ (b - r)}{\max - \min} + 120^\circ & \text{if } \max = g \\ \frac{60^\circ (r - g)}{\max - \min} + 240^\circ & \text{if } \max = b \end{cases} \quad (4)$$

$$S = \begin{cases} 0 & \text{if } \max = 0 \\ 1 - \min / \max & \text{otherwise} \end{cases}$$

$$B = \text{Max} \cdot B_{\max}$$

[View Source](#)

where  $r$ ,  $g$ , and  $b$  are the  $R$ ,  $G$ , and  $B$  values, respectively, of a pixel scaled to the range from 0 to 1;  $\max$  is the maximum of  $r$ ,  $g$ , and  $b$ , and  $\min$  is the minimum.

##### 5) Standard Benchmark Stone Calibration Check:

To ensure consistency of opal grading, a set of standard opals are kept with the GDA. They are used to monitor the repeatability of the calibrated GDA measurements for the same opal over time. This is the most stringent test since it monitors the repeatability over the full dynamic range.

After calibration steps 1)–3) are successfully completed, the operator places at least two standard opals into the GDA, which are then scanned and analyzed. The following parameters are calculated for the standard opal: total flash, body tone brightness, body tone saturation, body tone hue, body tone lightness, POC, and directionality. These parameters are automatically compared to the averaged values of individual parameters obtained from the prior scanning of the same opals. This is to ensure the consistency of these measurements made at different times. If the percentage error of any one of these parameters is above the preset threshold, the calibration using the standard stone will be marked as “failed”; otherwise, the calibration will be deemed as “passed.” The

threshold for each parameter can be set individually using the GDA GUI. We used 10% as the calibration tolerance threshold for these parameters.

### **B. Image Capturing**

Before capturing opal images, a backlit image is acquired first by switching off the overhead and angled lights then turning on the back lighting underneath the rotation stage. The backlit image is segmented to retrieve the opal object from the rotation stage background. The segmented opal is then used to generate a region of interest (ROI) by creating a circular region using the longest axis of the detected opal, plus a reasonable buffer. The coordinates of the ROI can then be used as the parameters for the camera to capture images just within the ROI. This reduces the amount of time taken to capture the necessary multiple images and also reduces storage requirements.

To accurately assess an opal, it is scanned over the full range of viewing angles. These are  $0^{\circ}$ – $360^{\circ}$  of rotation and  $0^{\circ}$ – $90^{\circ}$  of tilt at  $10^{\circ}$  intervals in both rotation and tilt angles. By using two camera exposure settings and the overhead lighting for each rotation angle, 720 images are captured. At tilt angles  $60^{\circ}$  and  $80^{\circ}$ , the angled lighting is also used. With the two camera exposure settings, 144 more images are acquired (the purpose of this is for assessing POC, discussed in Section IV-E). Therefore, 865 images are captured for each opal.

Because an opal is normally thin, the 865 images are sufficient to cover the entire opal surface area and all viewing angles. It is important to note here that opals have a backing and as such the opals face is only considered for valuation. As verified in Section IV-C, the color measurement produced from the GDA is consistent with that of a human observer. While the human observation results can be subjective, the GDA results are objective and repeatable. Therefore, rotating the opal through the third axis in the GDA is not necessary. This will result in excessive and duplicated images, which will not only unnecessarily inflate capture time, but also lead to excessive image processing time.

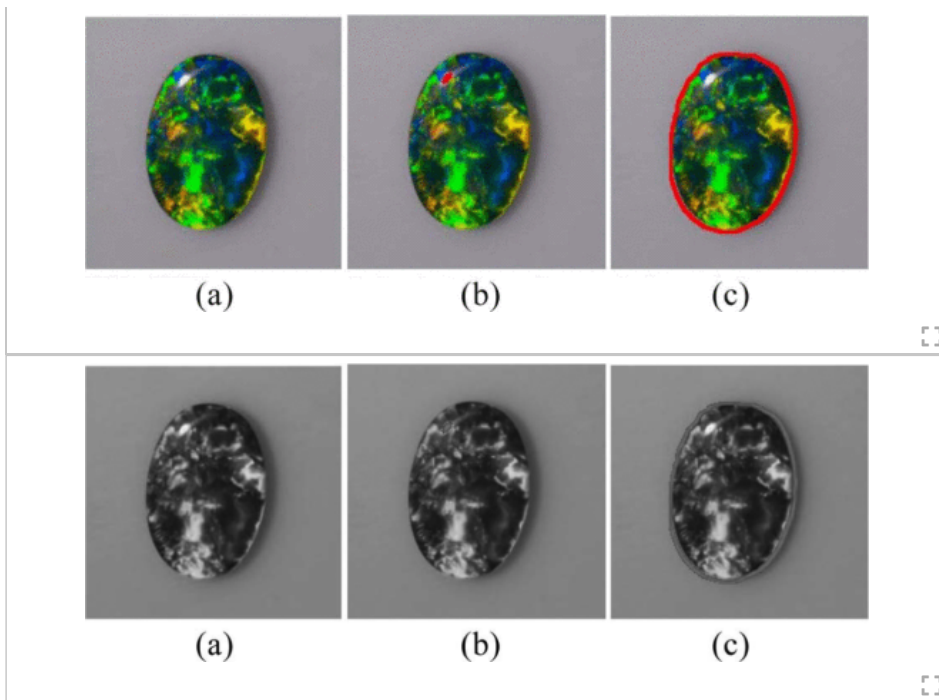
## **SECTION IV.** **Feature Extraction**

Having calibrated all the images captured at the multiple viewing angles, the next step is to carry out image analysis to extract the important features of the opal to be assessed. The image analysis as previously reported in [31] includes segmentation, flash histogram measurement, directionality, body tone, POC measurement, etc.

### **A. Segmentation**

Before any measurement can take place, the image must be segmented, i.e., the glint on the surface of the stone must be located and the stone must be separated from the background. The glint is a term used by gem appraisers. It is a small bright flash of light reflected from the shiny surface of an opal. The “glint” corresponds to the imaging term “specular highlight.” The glint spot on the opal surface is caused by specular reflection of the light source and needs to be detected and removed from further analysis. The detection is based on the lightness image generated from the sum of the three channels of the sRGB image. By restricting the pairwise difference of the three channels to be less than an empirically determined value, we can ensure that the regions detected are white rather than colorful. The values of the glint spot in the lightness image are higher than in other areas, therefore, the glint spot can be segmented by thresholding the lightness image [32].

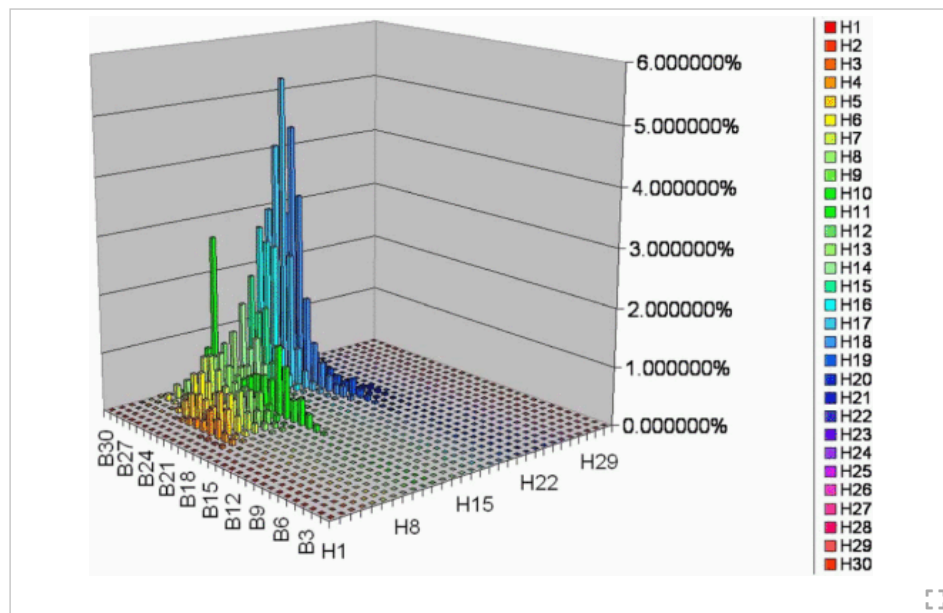
To segment the opal from the background, we use tone-mapped images rather than the extended dynamic range images. The tone-mapped images are produced using a nonlinear look-up table that maps the pixel values to unsigned char, compressing high-pixel values and enhancing the contrast in the darker areas of the opal. The difference between these images and similarly transformed images for the bare stage with no opal, is calculated, and the difference is used to construct an sRGBcor image. The opal segmentation is performed by applying a series of mathematical morphology operations on the image. This includes a morphological opening followed by a closing to suppress local noise, and finally a watershed process [33]. Fig. 7 shows the raw image, segmented glint, and segmented opal.

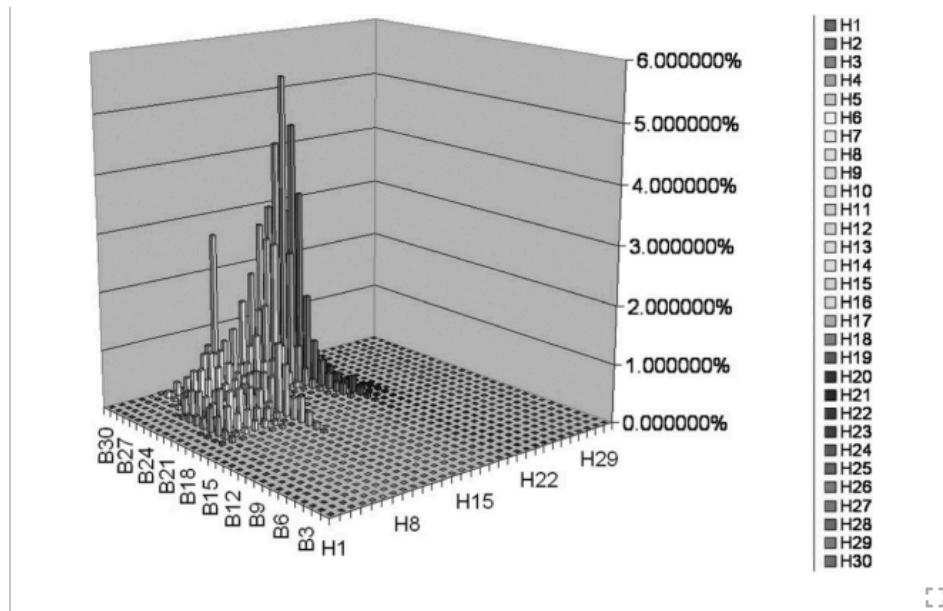


**Fig. 7.** Segmentation. (a) Raw image. (b) Segmented glint. (c) Segmented opal.

### B. Flash Histogram and Directionality Measurements

The flash is the color within a precious opal caused by refraction from the lattice of silica spheres. For each image, we have identified a stone mask which excludes the background and glint regions. We do not attempt to exclude “nonopal” regions such as rocks or body tone regions because these are only established at one tilt angle. The flash histogram measurement is a summary of the flash in histograms of standard HSB (sHSB). We create a summary of the stone color characteristics by taking a histogram of sHSB values present within the mask. Each histogram is a 3-D array of the counts of pixels falling within bins of HSB values. There are 30 hue bins linearly spaced in the range of  $0^\circ$ – $360^\circ$ . Saturation has ten bins between  $S$  flash ( $\sim 40\%$ ) and 100%, it is constrained to lie above the  $S$  flash threshold to exclude any faint glint that is not detected by our glint detectors. This will not exclude any flash because it is highly saturated. Note, however, that some nonflash regions may be excluded by the  $S$  flash threshold. Brightness has 30 bins piece-wise linearly spaced to give ten bins in the range containing body tone ( $0$ – $B$  flash) and 20 bins in the range containing strong flash ( $B$  flash– $B$  max). Fig. 8 shows a 3-D histogram of hue and brightness for a single saturation plane.



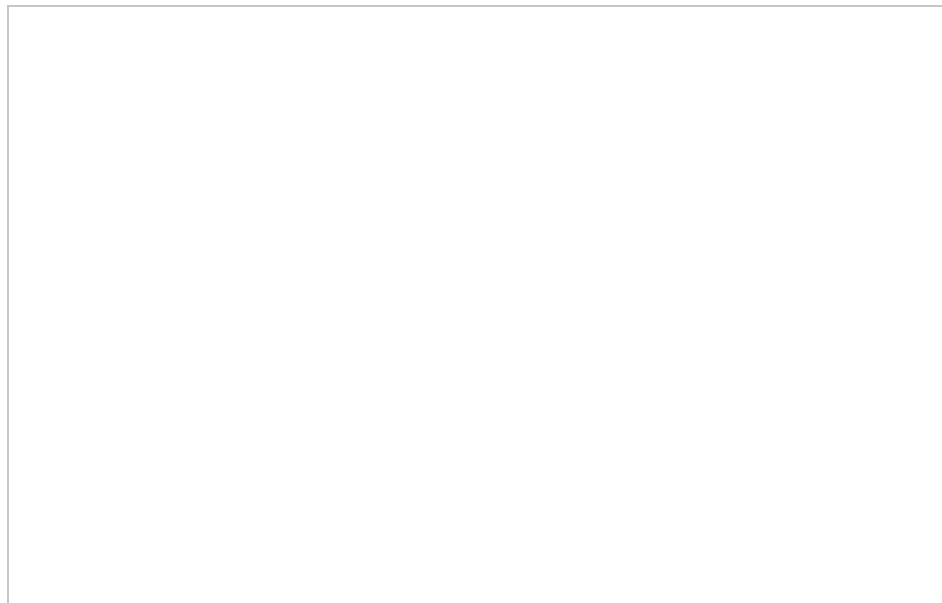


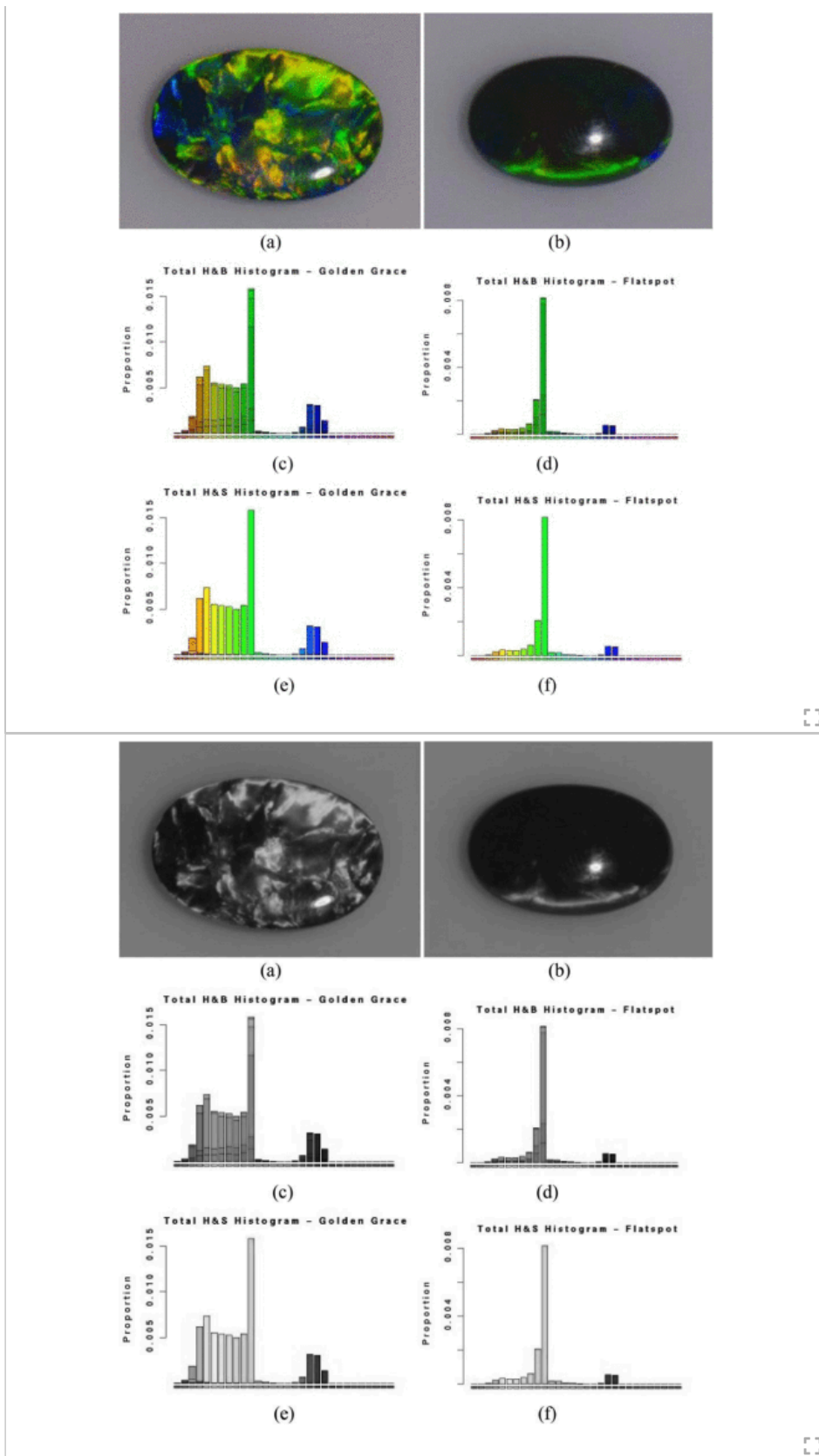
**Fig. 8.**

Three-dimensional histogram of hue and brightness for a single saturation plane.

The pixel count in each bin is normalized to the number of pixels in the stone (including glint regions), so the bin value gives the proportion of the stone having the HSB values of that bin. This histogram representation is a very compact summary of the color information. For example, a single opal image may be  $800 \times 800$  pixels. This requires 640 000 HSB values to store and display the color information. By discarding the spatial context, the 3-D histogram requires only 9000 bins ( $30 \text{ H bins} \times 10 \text{ S bins} \times 30 \text{ B bins}$ ) to store this information. Also, because we have discarded the spatial context, we can add the histograms from multiple views to get the average proportions of the stone having specific HSB values.

The summary 3-D stone histogram contains bin counts for both flash and body tone regions of the stone. We can separate these out by using the property that strong flash is both bright  $B > B_{\text{flash}} (500)$  and quite highly saturated  $S > S_{\text{flash}} (40\%)$ . The result is a 3-D histogram of flash HSB values, which can be stored, but is difficult to display for easy human interpretation. Consequently, we first combine all the Saturation bins and create a 2-D summary histogram of hue and brightness values. We also combine all the brightness bins and create a 2-D summary histogram of hue and saturation values. Summary H&B histograms and H&S histograms for two stones, “golden grace” and “flatspot,” are shown in Fig. 9.





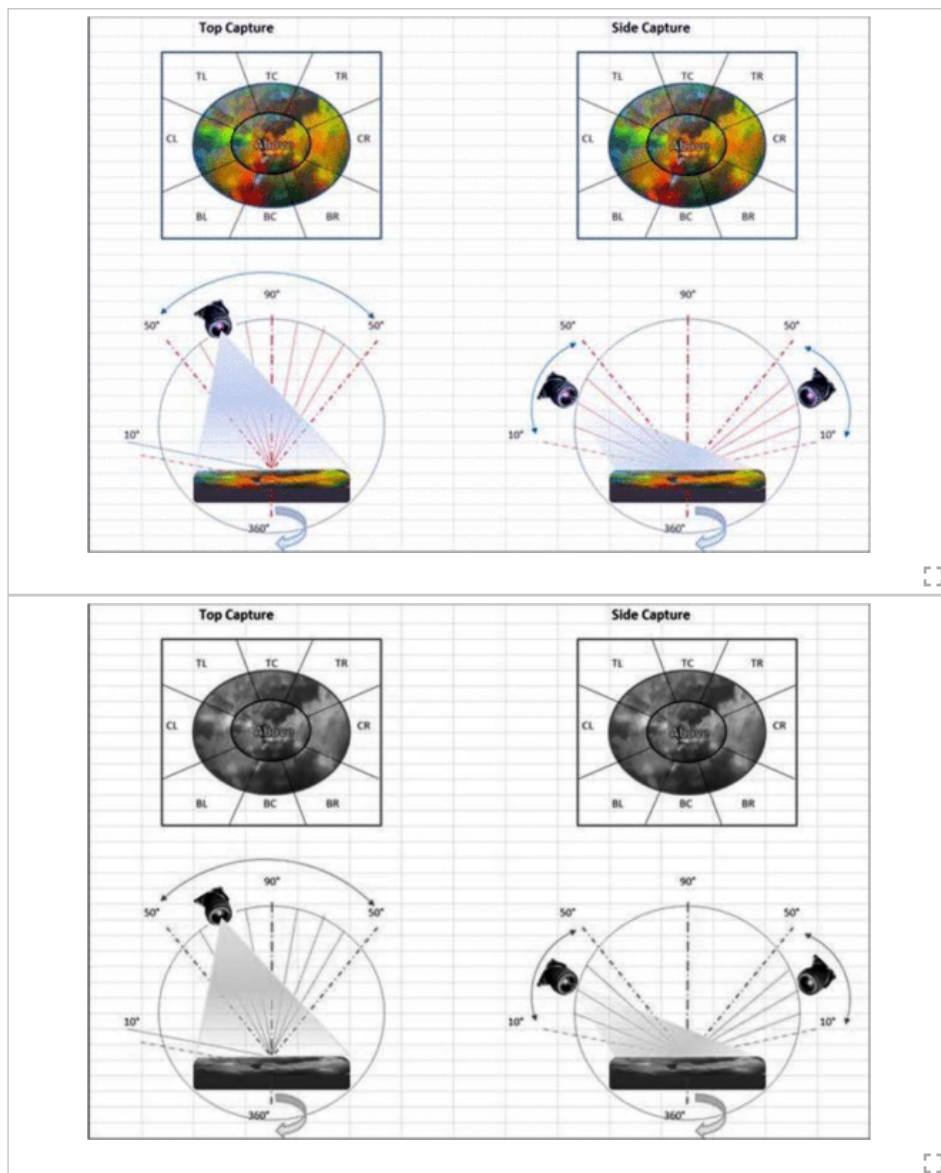
**Fig. 9.**

Summary hue and brightness histograms and hue and saturation histograms for two stones. (a) Golden grace and (b) flatspot taken at 80° tilt angle. (c) and (d) Hue and brightness histograms for the golden grace and the flatspot, respectively. (e) and (f) Hue and saturation histograms for the golden grace and flatspot, respectively.

The H&B histogram is to be interpreted as follows. Hue is plotted on the  $x$ -axis; the height of each histogram bar is the area proportion of that hue; within each bar, gradations of brightness are used to display the proportions of the area belonging to the various brightness bins for that hue. Similarly, the H&S histogram is to be interpreted as follows. Hue is plotted on the  $x$ -axis; the height of each histogram bar is the area proportion of that hue; within each bar, gradations of saturation are used to display the proportions of the area belonging to the various saturation bins for that hue. Note that these gradations are not as informative because flash does not tend to vary in saturation very much.

Note that according to the summary H&B histograms in Fig. 9, the maximum area proportion of a single hue in golden grace is only about twice that of flatspot. However, when we examine the images (taken at  $80^\circ$  tilt angle), it is obvious from where the flatspot stone gets its name. There is a flat spot in its flash when viewed from above. This information is not at all evident in the summary histogram. For this reason, we have produced nine additional H&B histograms to summarize this directional information.

To calculate the total flash, we need to add the top flash and the side flash. Both flashes are the summation of all histogram bins, namely, H&B histograms for all ten saturation planes. The top flash is the total flash calculated using the images acquired with rotation stage tilt angles  $50^\circ$ ,  $60^\circ$ ,  $70^\circ$ ,  $80^\circ$ , and  $90^\circ$ . The side flash is the total flash calculated using the images acquired with rotation stage tilt angles  $0^\circ$ ,  $10^\circ$ ,  $20^\circ$ ,  $30^\circ$ , and  $40^\circ$ . Fig. 10 illustrates how the top flash and side flash are summarized. The figure also shows the relative camera and opal positions, although in reality it is the stage which tilts and rotates while the camera remains fixed.





**Fig. 10.**

Opal flash summarization. (Top) The images captured at 10° rotation interval are summarized into eight sectors (TL and TR). (Bottom) The images captured at 10° tilt interval are summarized into top (BL) and side (BR) views.

The total flash can be formulated as follows:

$$\text{Flash} = \sum_{s=1}^{10} \sum_{b=1}^{30} \sum_{h=1}^{30} (\text{HistTop}_{s,b,h} \text{WeightTop}_{s,b,h}) + \sum_{s=1}^{10} \sum_{b=1}^{30} \sum_{h=1}^{30} (\text{HistSide}_{s,b,h} \text{WeightSide}_{s,b,h}) \quad (5)$$

[View Source](#)

where  $s = 1, \dots, 10$  represent all ten saturation planes,  $b = 1, \dots, 30$  represent all 30 brightness histogram bins, and  $h = 1, \dots, 30$  represent all 30 hue histogram bins.  $\text{HistTop}_{s,b,h}$  is the summation of the bin values shown in Fig. 8, over the nine different directional viewing angles as listed in Table I. They include above, bottom center (BC), bottom right (BR), center right (CR), top right (TR), top center (TC), top left (TL), center left (CL), and bottom left (BL). Similarly,  $\text{HistSide}_{s,b,h}$  is the summation of the bin values of BC, BR, CR, TR, TC, TL, CL, and BL. Equations (6) and (7) define the  $\text{HistTop}_{s,b,h}$  and  $\text{HistSide}_{s,b,h}$ .  $\text{WeightTop}_{s,b,h}$  are the weights assigned to individual hue versus brightness bins for each saturation plane using the images acquired with the rotation stage tilt angles 50°, 60°, 70°, 80°, and 90°. Similarly,  $\text{WeightSide}_{s,b,h}$  are the weights assigned to individual hue versus brightness bins for each saturation plane using the images acquired with the rotation stage tilt angles 0°, 10°, 20°, 30°, and 40°

$$\begin{aligned} \text{HistTop}_{s,b,h} = & \text{HistAbove}_{s,b,h} + \text{HistBC}_{s,b,h} + \text{HistBR}_{s,b,h} \\ & + \text{HistCR}_{s,b,h} + \text{HistTR}_{s,b,h} + \text{HistTC}_{s,b,h} \\ & + \text{HistTL}_{s,b,h} + \text{HistCL}_{s,b,h} + \text{HistBL}_{s,b,h} \end{aligned} \quad (6)$$

[View Source](#)

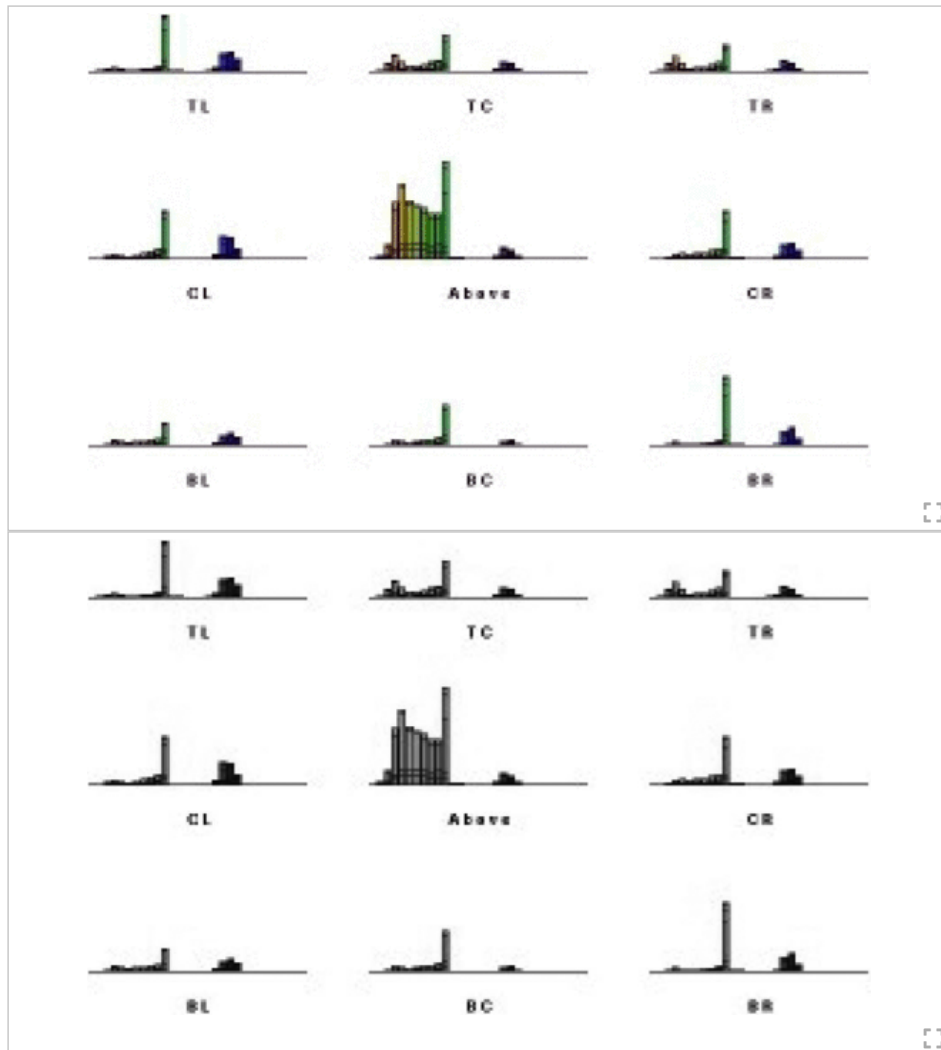
$$\begin{aligned} \text{HistSide}_{s,b,h} = & \text{HistBC}_{s,b,h} + \text{HistBR}_{s,b,h} + \text{HistCR}_{s,b,h} \\ & + \text{HistTR}_{s,b,h} + \text{HistTC}_{s,b,h} + \text{HistTL}_{s,b,h} \\ & + \text{HistCL}_{s,b,h} + \text{HistBL}_{s,b,h}. \end{aligned} \quad (7)$$

[View Source](#)

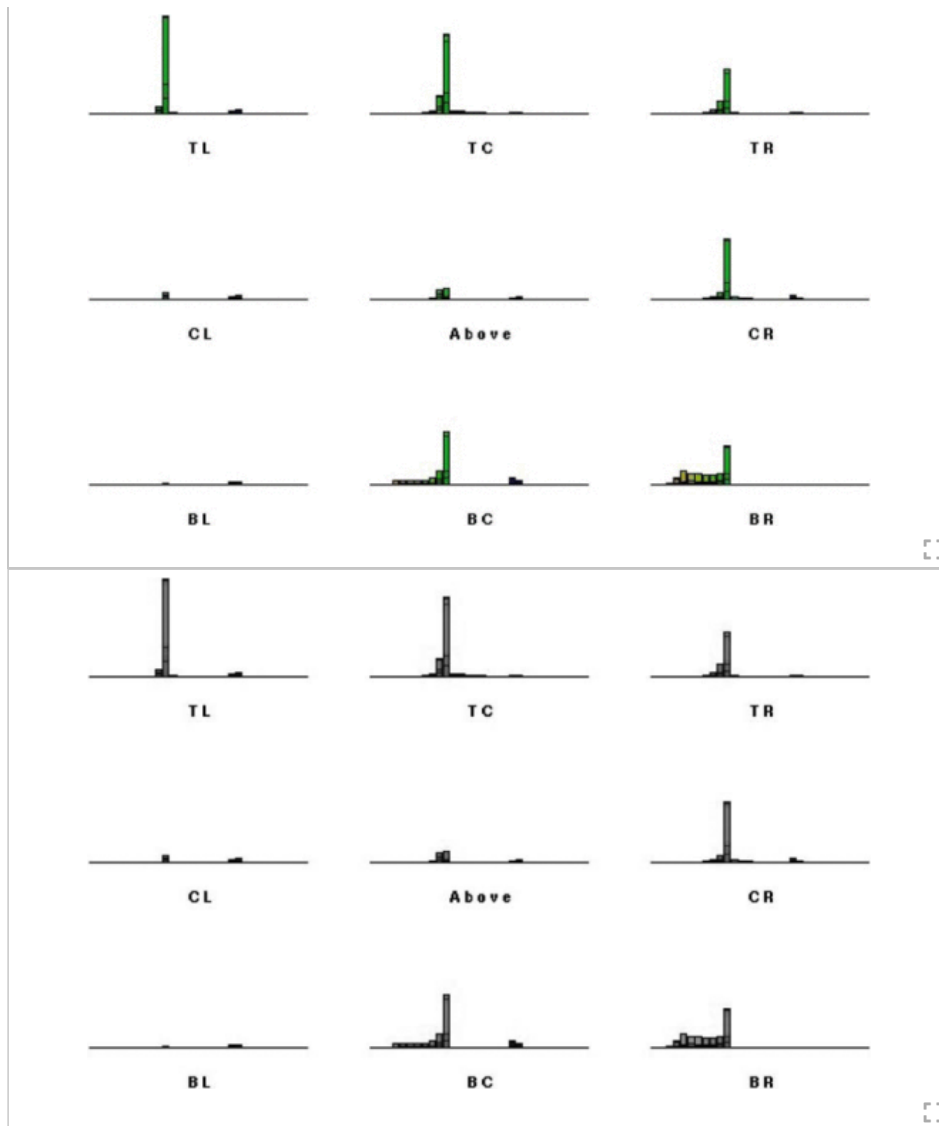
**TABLE I** Definition of Viewing Angle Ranges for Directional Histograms (Tilt is the Stage Tilt Angle and ROT is the Stage Rotation Angle)

|                    |  |
|--------------------|--|
| Above              | ( $\text{tilt} > 60^\circ$ )   |
| BC - bottom centre | ( $\text{tilt} \leq 60^\circ$ ) & (( $\text{rot} > 337.5^\circ$ )    ( $\text{rot} \leq 22.5^\circ$ )) |
| BR - bottom right  | ( $\text{tilt} \leq 60^\circ$ ) & (( $\text{rot} > 22.5^\circ$ ) & ( $\text{rot} \leq 67.5^\circ$ ))   |
| CR - centre right  | ( $\text{tilt} \leq 60^\circ$ ) & (( $\text{rot} > 67.5^\circ$ ) & ( $\text{rot} \leq 112.5^\circ$ ))  |
| TR - top right     | ( $\text{tilt} \leq 60^\circ$ ) & (( $\text{rot} > 112.5^\circ$ ) & ( $\text{rot} \leq 157.5^\circ$ )) |
| TC - top centre    | ( $\text{tilt} \leq 60^\circ$ ) & (( $\text{rot} > 157.5^\circ$ ) & ( $\text{rot} \leq 202.5^\circ$ )) |
| TL - top left      | ( $\text{tilt} \leq 60^\circ$ ) & (( $\text{rot} > 202.5^\circ$ ) & ( $\text{rot} \leq 247.5^\circ$ )) |
| CL - centre left   | ( $\text{tilt} \leq 60^\circ$ ) & (( $\text{rot} > 247.5^\circ$ ) & ( $\text{rot} \leq 292.5^\circ$ )) |
| BL - bottom left   | ( $\text{tilt} \leq 60^\circ$ ) & (( $\text{rot} > 292.5^\circ$ ) & ( $\text{rot} \leq 337.5^\circ$ )) |

Directional histograms of the flash hue and brightness values are also calculated to show the flash of an opal when viewed from different directions. Table I defines the range of viewing angles that have been combined for each of the histograms. Figs. 11 and 12 show the directional hue and brightness histograms for the two opals, golden grace and flatspot, respectively. The directional histograms for flatspot clearly show that there is very little flash when viewed from above, but it has strong green flashes when viewed from the TL direction. By contrast, the directional histogram for golden grace shows that it displays the largest area of flash and is also most colorful (flashing orange, gold, and green) when viewed from above. This directional information is important for buyers when choosing an opal for a jewelry setting which has specific directionality constraints, such as a pendant or brooch, rather than for a ring which can be easily viewed from many directions.



**Fig. 11.** Directional hue and brightness histograms for the golden grace.



**Fig. 12.** Directional hue and brightness histograms for the flatspot.

The opal directionality measurement can be depicted as below

$$\text{Directionality} = \frac{\text{TopDirectionality} + \text{SideDirectionality}}{2}. \quad (8)$$

[View Source](#)

The TopDirectionality is the average value of the normalized total histograms for the nine different directional viewing angles as shown in Table I. Similarly, SideDirectionality is the average value of the normalized total histograms for BC, BR, CR, TR, TC, TL, CL, and BL. The TopDirectionality and SideDirectionality can be formulated as below

$$\begin{aligned} &\text{TopDirectionality} \\ &= \frac{1}{9} \sum_{i=1}^9 \frac{\text{HistTop}D_i}{\text{Max}(\text{HistTop}D_1, \text{HistTop}D_2, \dots, \text{HistTop}D_9)} \end{aligned} \quad (9)$$

$$\begin{aligned} &\text{SideDirectionality} \\ &= \frac{1}{8} \sum_{i=1}^8 \frac{\text{HistSide}D_i}{\text{Max}(\text{HistSide}D_1, \text{HistSide}D_2, \dots, \text{HistSide}D_8)} \end{aligned} \quad (10)$$

[View Source](#)

where  $\text{HistTop}D_i$  and  $\text{HistSide}D_i$  can be calculated using the following formulas:

$$\text{HistTop}D_i = \sum_{s=1}^{10} \sum_{b=1}^{30} \sum_{h=1}^{30} \text{HistTop}_{s,b,h} \quad (11)$$

$$\text{HistSide}D_i = \sum_{s=1}^{10} \sum_{b=1}^{30} \sum_{h=1}^{30} \text{HistSide}_{s,b,h} \quad (12)$$

[View Source](#)

### C. Validation of Color Measurement

Two aspects of the GDAs color measurement are experimentally validated. The first aspect concerns the repeatability of the measurements. Having repeatable hue measurements is critical to the objectivity of the GDA. The major source of variability in this regard is the manual placement of the opal on the stage. If an opal is processed by the GDA, removed and then randomly placed back on the stage, we cannot guarantee that the images produced will be identical for each process. This is because the viewing angles are sampled in increments of  $10^\circ$  in rotation and tilt. The output color histograms were compared both visually and using a statistical similarity measure [34].

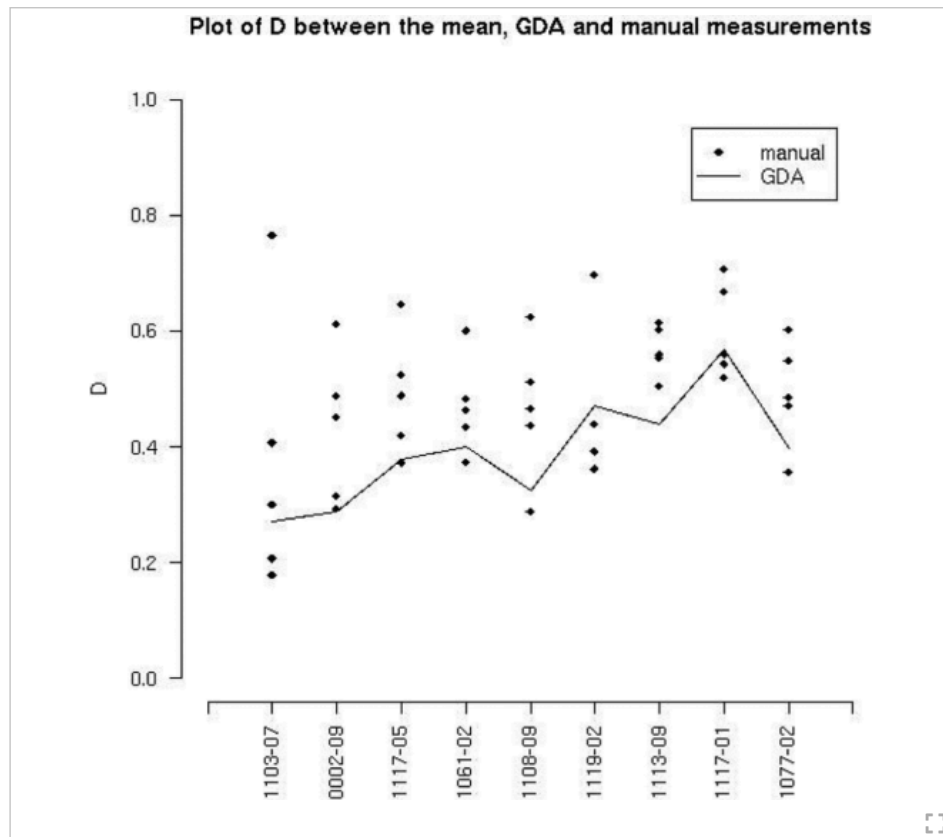
The second validation aspect is the consistency of the GDA output with that of a human observer. To experimentally validate that such consistency is achieved, GDA results were compared to human assessments. This comparison was done over a number of marker opals, which were representative of the following opal classes: black, dark, boulder, and white. Each of these opals was manually assessed by five experienced human assessors and histograms of color were produced. The five human graders were asked to manually grade the opals by annotating their hue characteristics in a form comparable to that produced by the GDA. The annotation was based on comparisons between the observed flash regions in the opal and a color chart with labels for each of the hues. Because filling in entries for each cell in a  $30 \times 30 \times 10$  histogram of brightness, hue, and saturation, as described in (6) and (7), would be very difficult for the human graders, they were asked only to provide entries for hue. Typically, a manual grading would produce a 1-D hue histogram, with area proportion estimates in around four or five out of the 30 bins. A mean histogram of the manual measurements was in turn computed by averaging multiple observations for the same opal. A statistical measure, namely the pair wise histogram similarity measure [34],  $D$ , was used to measure the difference between the GDA produced histograms for multiple evaluations of the same opal, and the mean histogram of these histograms. Similar distances were computed between the manually generated histograms and their mean histogram. Let us denote a histogram of hue for an opal "A" by  $\text{hist}_A(h)$ , where  $h$  is the 30 hue values. The histogram similarity measure  $D$  can then be depicted by (13). Here  $\text{Fhist}_A(h)$  is defined in (14), where  $\text{Fhist}$  is a "fuzzy set" associated with  $\text{hist}$ , which is obtained by dividing each  $\text{hist}$  value by the histogram's maximum. Values of  $D$  close to 1 represent a large distance between histograms. Values near zero indicate high similarity

$$D(A, B) = \frac{\sum_{h=1}^{30} |\text{Fhist}_A(h) - \text{Fhist}_B(h)|}{\sum_{h=1}^{30} (\text{Fhist}_A(h) + \text{Fhist}_B(h))} \quad (13)$$

$$\text{Fhist}_A(h) = \frac{\text{hist}_A(h)}{\max(\text{hist}_A(h))}. \quad (14)$$

[View Source](#)

Fig. 13 shows a plot of these distance values. The horizontal axis shows the delivery numbers of individual opals used in the experiment, such as 1103-07 and 0002-09. It can be seen that the values of  $D$  for the GDA produced measurements are within the range of the  $D$  values corresponding to the manual measurements. The figure shows that the GDA is producing results that are consistent with manually generated data.



**Fig. 13.**

Plot of difference between mean, GDA, and manually generated histograms for various opals.

#### D. Body Tone

In order to measure the body tone of a stone, we must first find the viewing angle at which the body tone is most readily visible. We avoid using the  $90^\circ$  stage tilt angle because this geometry often produces a large area of surface glint. The lower the stage tilt angle, the less of the stone surface is visible. So an  $80^\circ$  stage tilt angle is optimal. From the flash histograms, we can determine which rotation angle shows the smallest area of strong flash. This rotation angle,  $rotMinFlash$ , should have the largest area of body tone.

Previously we have segmented the stone and excluded the glint regions and, in the case of crystal opals, excluded the internal opaque regions since these will interfere with the measurement of the body tone of the crystal. Now, we need to determine the regions within the stone mask which display body tone before we can measure the color characteristics of that body tone. Firstly we remove the strong flash regions from the stone mask by excluding all pixels with  $Brightness > Bflash$ . We will then be left with nonflash regions within the stone.

If the stone only has opal in its face, then the body tone regions will be those where the flash is completely “turned off” i.e., the darkest part of the nonflash regions. Unfortunately this simple definition of body tone region is not valid in all cases. If the stone has either potch (opal without the crystal structure which causes flash) or boulder (the rock in which the opal is embedded) present in the face, then the darkest part of the stone may well belong to these “nonprecious opal” regions rather than to the body tone of the opal present in the face.

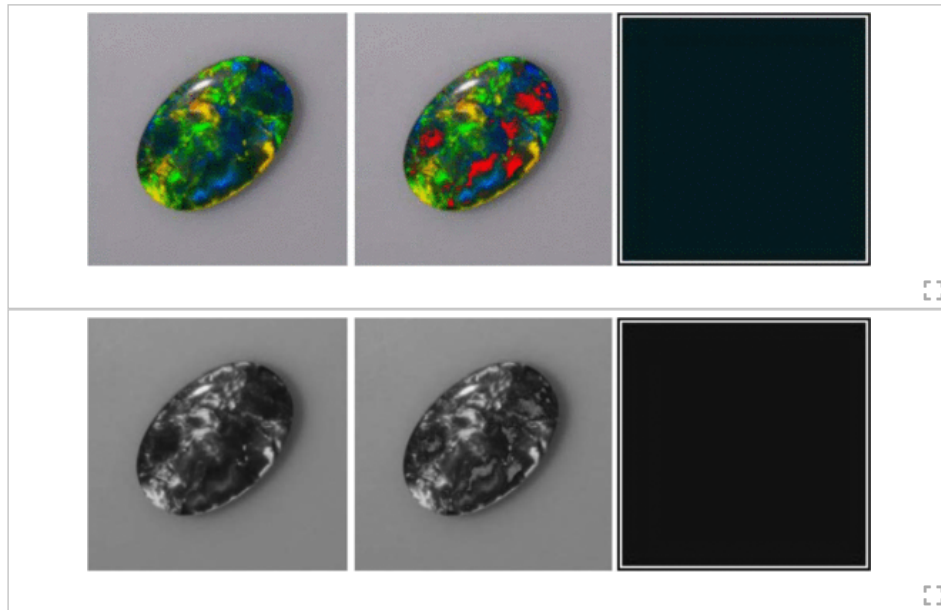
To allow for the possibility of mixed-face opals, we search for two color clusters,  $cluster_0$  and  $cluster_1$ , in the nonflash regions of the stone. We present to the operator the average color of the darkest 20% of both clusters and the regions they occupy within the stone. We then allow the operator to select the cluster containing the body tone. If the stone only has colored opal in the face, then these two clusters will typically be body tone and dark flash. If the stone has colored opal and potch in the face, then the two clusters will typically be body tone and potch. If the stone has opal and boulder in the face, then the two clusters will typically be body tone and boulder.

Having determined the body tone region in the image, we take the mean or average sRGB values within this region, and convert these to HSB values. Unlike the flash histograms which separate hue, brightness, and saturation into discrete bins, the body tone is expressed as continuous values. Body tone hue lies in the range of  $0^{\circ}$ – $360^{\circ}$  and is scaled to give a hue number (HN) between 0.0 and 30.0. Body tone brightness is scaled to give a brightness number (BN) between 0.5 and 10.5, for the darkest and brightest stones respectively. Body tone saturation is scaled to give a saturation number (SN) between 0.5 and 10.5, for the blackest and whitest stones, respectively.

We also provide an additional measure of the body tone by calculating the lightness, which is the average of the sRGB values. This is scaled to give a lightness number (LN) between 0.5 and 10.5, for the darkest and brightest stones, respectively. So, for cluster0, sRGBcls0 is converted to HNO, BNO, SNO, and LNO. Similarly, for cluster1, sRGBcls1 is converted to HN1, BN1, SN1, and LN1.

To determine the body tone color, a choice is made between the two candidate body tone clusters, cluster0 and cluster1, based on rules appropriate to the opal's class. For a black opal, dark flash is lighter than the body tone, so we select the darker of the two clusters as body tone. The same is true for crystal opals. It is the opposite for a white opal, the lighter of the two clusters is selected as its body tone. The same principle applies to the boulder opals. For a dark opal, if the brightness of one of two clusters is greater than 4.5, the principle for the white opals applies; otherwise the principle for the black opals should apply.

We then report the HN, SN, BN, and LN values of the body tone as shown in Fig. 14.



**Fig. 14.** Body tone measurement. Opal image (left), body tone region shown in red (center), swatch showing the body tone color (right) with HN = 15.75, SN = 0.74, BN = 2.2, and LN = 1.62.

### E. Play of Color

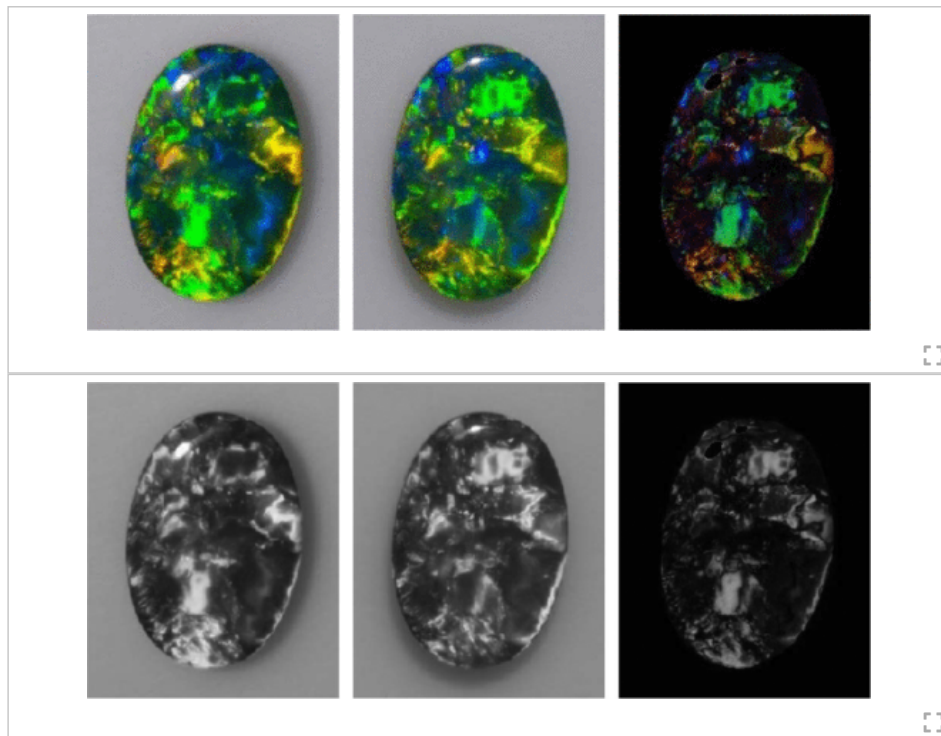
The histograms described previously are a summary of the areas of flash displayed at various viewing angles. The directional histograms are a summary of whether the flash changes in area, HSB with viewing angles. These histograms do not take into account the spatial location of the flash. If the flash changes position between viewing angle changes, but retains the same area and color, there will be no change in the histograms at these angles. This phenomenon of flash of a specific color changing position, or a specific region of flash changing color, as the viewing angle is changed, is termed POC. To measure this attribute, we need to compare images taken with different viewing angles.

Geometric distortion of the stone will be present if we attempt to compare images from different stage tilt angles. Therefore it is preferable to compare images taken at different stage rotation angles, or different lighting angles, for a given stage tilt angle. Because we are after an overview of

the POC, a sampling frequency of  $20^\circ$  is considered adequate in both rotation and tilt angles. POC is generally taken to be a characteristic of the above view of the stone (i.e.,  $50^\circ$ ,  $60^\circ$ ,  $70^\circ$ ,  $80^\circ$ , and  $90^\circ$  stage tilt angles). We also wish to avoid the  $90^\circ$  tilt angle because it produces a large area of surface glint areas. We therefore sample images at the tilt angles of  $60^\circ$  and  $80^\circ$ .

Images taken at different stage rotation angles must be rotated back in software in order to align them before they can be compared. This step is not necessary if different lighting angles are used. However, if different lighting angles are used, then each separate light source must have its own set of color calibration files. The latter option of a secondary forward lighting source has been implemented in the GDA.

A POC measure must detect both presentations of POC—change of color or change of position. There are several ways of doing this. One simple method is to take the average of the absolute difference of the two co-registered views for the series of rotation and tilt angles. An example of two lighting angle images and their difference image are shown in Fig. 15. The difference image shows the POC. The difference image is computed simply by subtracting the  $R$ ,  $G$ , and  $B$  values of a pixel of the left image from the  $R$ ,  $G$ , and  $B$  values of the corresponding pixel of the middle image. The absolute differences of the  $R$ ,  $G$ , and  $B$  values are used as the  $R$ ,  $G$ , and  $B$  values of the corresponding pixel of the difference image, shown at the right in the figure. By doing the pixel-wise subtractions, the difference image can be constructed. At a single rotation angle, the “difference” score is defined as the sum of the average absolute difference within the stone mask (excluding the glint masks) of the two co-registered views for the red, green, and blue bands of the SRGB images.



**Fig. 15.**

Two lighting angle images (left and middle) and their difference image (right) showing POC with a POC value of 69.08.

If a flash region changes color between the two views, then the difference score will detect it. Larger color changes will give a higher difference score, as will larger areas of color change. If a specific flash region moves position but not color, then the difference score will also detect this. The score can be scaled to have a range of 0 to 100 by dividing by the difference score of the marker stone with the greatest POC and multiplying by 100.

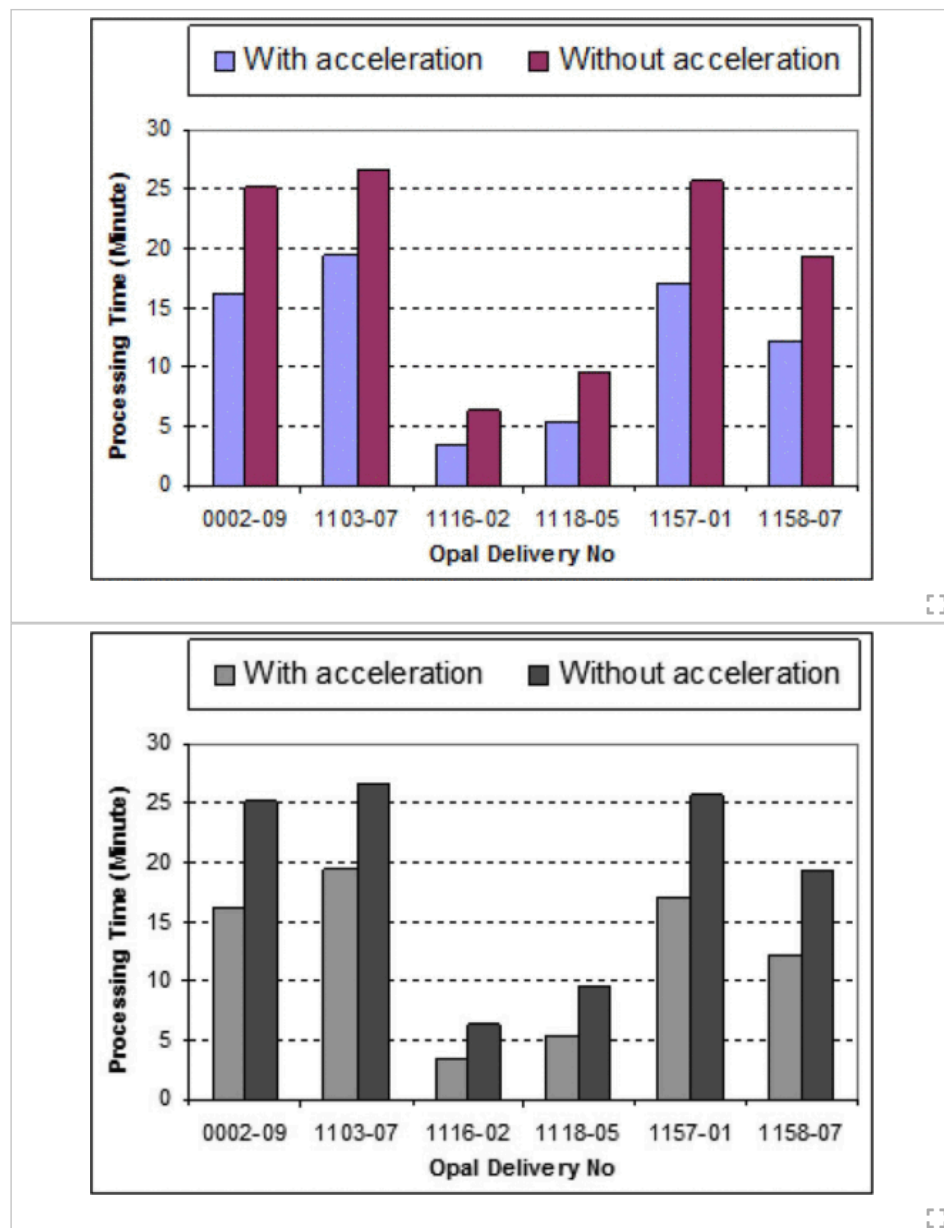
#### **F. Accelerated Image Processing**

For each opal, 865 images are captured. Processing such an amount of images is both a data and computationally intensive task. It takes an average of 20 min to produce opal quality measurements even on a high-end computer.

With the progress in computing power, computers with multicore CPUs are now becoming standard. However, a multicore CPU does not speed up any application automatically. To tackle the data and compute-intensive image processing problem, we have employed a shared-memory parallel image processing model to take advantage of the multicore processing power.

To accelerate the image processing, the OpenMP application program interface is employed. It supports multiplatform shared-memory parallel processing and provides a simple and flexible interface for developing parallel applications. To parallelize the time consuming image analysis functions, we apply OpenMP directives to the parallelizable blocks of these functions [35]. The MS Visual Studio C++ compiler will use the directives to create a multithreaded executable.

To test the GDA performance with the accelerated image analysis module, experiments were conducted on a Dell Precision T5400 workstation with a quad-core Intel Xeon processor (2.5 GHz) and 4 GB RAM. Test samples include six opals with different classes and sizes. Fig. 16 shows the comparison of the GDA performance before and after the acceleration was implemented. With the accelerated image analysis, the image processing time for each opal has been reduced by about 36% [36].





**Fig. 16.**

Comparison of the GDA performance with and without the acceleration.

---

## SECTION V.

# Automated Opal Classification and Grading

The goal of the GDA is to automatically grade an opal by quantifying the color characterization of the opal, including flash, body tone, POC, etc.

The company, Opal Producers Australia Ltd., has carried out an extensive industry survey, to gather data from 60 experienced opal assessors with over 20 years of experience each in the industry, for a range of opal classes. Development work was required to link the GDA measured data with the information from the industry survey, to provide guidelines and the foundation for the successful comparison of grading results. Opal grading is a highly nonlinear problem in regard to the relationship between the opal grade and the opal's characteristics; it has been an industry challenge to find a solution to the problem. Prior to the implementation of the statistical learning-based grading, we undertook a comprehensive analysis to identify important opal features and formulate the relationship between the GDA gem score of an opal and its characteristics. Due to the complexity of opal grading, it is very hard to build a formula-based model to grade opals. We instead have used machine learning approaches.

### A. Statistical Machine Learning

SML is used in automated opal grading. SML is a group of modern machine learning methodologies which merge statistics with the computational sciences including computer science, systems science, and optimization. The internal representation of SML is a statistical model that learns from observed data and is then used for making decisions and predictions [37]. A support vector machine (SVM) is one type of supervised learning algorithm which is based on SML theory [38]– [41]. It has made statistical learning theory not only a tool for theoretical analysis but also a tool for creating practical algorithms for classification and regression. There are two excellent tutorials which detail the classification [42] and regression problems [43].

For the SVM for classification (SVC), it takes a set of training data, with each observation marked as belonging to one of the classes of interest. A SVM training algorithm builds a model that assigns a new example into one of these classes. The SVM model is a representation of the training data as points mapped in a high-dimensional feature space, so the training data of all classes are separated by a clear gap that is as large as possible. The new examples are also mapped into the same space and predicted to belong to one of the classes based on which side of the gap they fall on. Theoretically, the training is a process to construct a hyperplane which optimally separates the training data into their classes. The points spanning the hyperplane are the support vectors.

When a SVM is used for resolving regression problems, it is called SVR. In this case, it uses a series of training examples to build a decision maker system which predicts new values. Many of the basic ideas of the SVC carry directly over to the SVR, with only a few differences, including: 1) the output of the SVR is a real number instead of a class label, the real number has infinite possibilities and 2) the training of a SVR is learning a function, and it is a process of minimizing the error between the predicted value and the real value of a training example. However, maximizing margins among the classes is the goal in the training of an SVC.

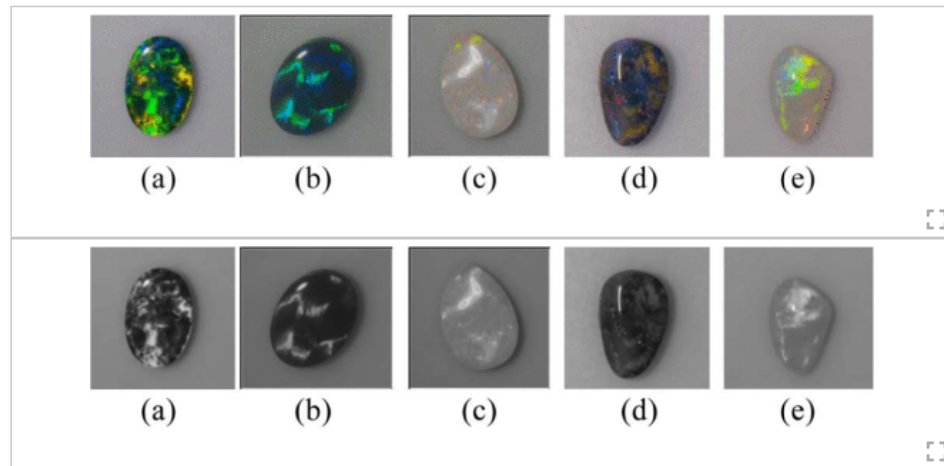
The two key elements in the SVM, including both SVC and SVR, are: 1) a general-purpose learning machine, and 2) a problem specific kernel function, which can be a linear, polynomial, sigmoid, or RBF. The flexibility of these kernel functions enables the SVM to explore a wide variety of hypothesis spaces. SVMs can be formulated with two things: hypothesis spaces and loss functions. By training, SVMs find an optimal hyperplane as the solution to a learning problem.

SVMs have been used widely in various applications. For the classification case, SVMs have been used for face detection [44] in images, text categorization [45], etc. For the regression case, SVMs have been compared on benchmark time series prediction tests and have shown either similar or significantly better performance than that of competing methods [46].

### B. Automated Opal Classification

Since the class of an opal is an important feature for the opal assessment, and ultimately grading, it is critical to determine the class of an opal before the assessment and grading processes can be carried out.

The opal class is determined by the two common characteristics of body tone and transparency. Body tone is one of the most important factors in the classification of opals. It refers to the background or the underlying color of the opal, and ranges from black through dark (gray) to white. An opal can be classified into “black,” “dark,” or “white” based on its body tone. Opals also show all forms of diaphaneity ranging from transparent through translucent to opaque. If an opal is transparent or semi-transparent, it is classified as crystal opal. The term “crystal” refers to the appearance of the opal instead of its crystalline structure. Based on chemical composition and the homogeneity of opals, they can be classified into either “all opal” or “boulder.” The all opal means that an opal is presented in one piece, and is of substantially homogenous chemical composition. The term boulder is used when an opal is presented in one piece while naturally attached to the host rock in which it was formed. The host rock will have a different chemical composition. This type of opal is classified as boulder opal [1]. Fig. 17 shows sample opals of five different classes.



**Fig. 17.**

Sample opals from different classes. (a) Blank opal. (b) Dark opal. (c) White opal. (d) Boulder opal. (e) Crystal opal.

An opal can be categorized into one of five classes, namely, black, dark, white, crystal, and boulder. Both crystal and boulder types of opals are easily identified by the naked eye. The classes of these opals are directly entered into the GDA database. Therefore, the automated opal classification is for identifying black, dark, and white opals only.

The automated classification of an opal is based on its body tone measurement. The BN and SN of the two candidate body tone clusters,  $cluster_0$  and  $cluster_1$  are employed in the opal classification [47], [48]. These values together with the ground truth of the opal class form a training sample for an opal classifier based on a SVM. The sample opals from each class are selected to represent the entire range of opals of that class. Table II shows a sample training dataset for opal classification. 558 sample opals from different classes are used for training, and 423 sample opals from different classes are used for testing. The training dataset includes the same number of training samples for each opal class. Wherever practical, representative opal samples are selected for each class to reflect the actual distribution of the body tone of the class. The same principle is followed when selecting the testing samples to represent each opal class. No testing samples are used in the training.

**TABLE II** Sample Training Dataset for Opal Classification

| Opal Delivery No. | BNO  | SNO  | BN1  | SN1  | Class Label |
|-------------------|------|------|------|------|-------------|
| 1001-01           | 2.72 | 2.21 | 3.12 | 0.65 | 1 - Black   |
| 1002-05           | 2.4  | 5.03 | 3.48 | 1.85 | 1 - Black   |
| 1003-02           | 2.44 | 3.8  | 4.88 | 1.1  | 1 - Black   |
| 1019-08           | 3.82 | 5.44 | 5.7  | 0.92 | 2 - Dark    |
| 1024-09           | 3.8  | 2.38 | 4.64 | 4.9  | 2 - Dark    |
| 1054-10           | 4.34 | 7.58 | 6.2  | 4.18 | 2 - Dark    |
| 1156-08           | 6.06 | 8.71 | 7    | 8.75 | 3 - White   |
| 1103-07           | 5.98 | 9.51 | 6.22 | 8.96 | 3 - White   |
| 1156-04           | 6.82 | 8.72 | 6.88 | 8.71 | 3 - White   |

After the training, an SVM model is established to identify an opal's class. The successful classification rate is 90.35%. We find that some black opals are classified as dark, and some dark opals are classified as black or white. These misclassifications reflect the fact that some black and dark types of opals are hard to be categorized distinctly. The results also demonstrate that all white opals in the test set were classified correctly.

The parameters used in the SVM classification are as follows.

- 1) SVM type:  $N$ -class classification.
- 2) RBF kernel,  $d(x, y) = \exp(-\text{gamma}|x - y|^2)$ , where  $x$  and  $y$  are two feature vectors in the input space,  $|x - y|^2$  is the squared Euclidean distance between the two feature vectors, and  $\text{gamma} = 1$ .
- 3) The parameter  $\text{nu} = 0.9999$ . The larger this value, the smoother the decision boundary. The termination criterion is either 100 000 for the maximum iteration or 0.000001 for the epsilon in the insensitive-loss function, whichever is reached first.

Once the SVM is trained, it can be used to classify an opal. For example, after the opal, with delivery number 1157-01, is scanned and its images are analyzed, BNO, SNO, BN1, and SN1 are produced with the following values: 2.4, 0.71, 4.26, and 0.93. These values are then used as the inputs to the SVM model which will produce the class label 1 (black) for the opal. That is, the opal 1157-01 is classified as a black opal.


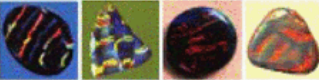



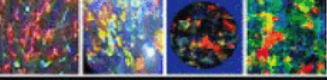
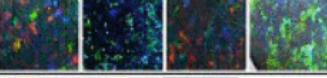
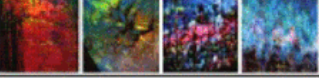
Comparing with the classification results from the skilled opal assessors, the GDA can classify over 90% of opals accurately into their correct classes. In the GDA data entry, prior to the opal classification by the GDA, an opal class has been manually entered based on the GDA operator's observation and experience and/or the information from the opal source. After an opal is automatically classified by the GDA, the opal class produced from the GDA is compared with the manually entered opal class. If they match, the opal can be graded using the automated grading procedure described in the following section. However, if the classes mismatch, validation is required for the operator to confirm either the GDA produced class, or the manually entered class shall be used in the opal grading. Over time, after more throughputs of opals and hence machine learning, the requirement for the operator validation to confirm the class of the opals in question could be gradually eliminated.

### C. Automated Opal Grading

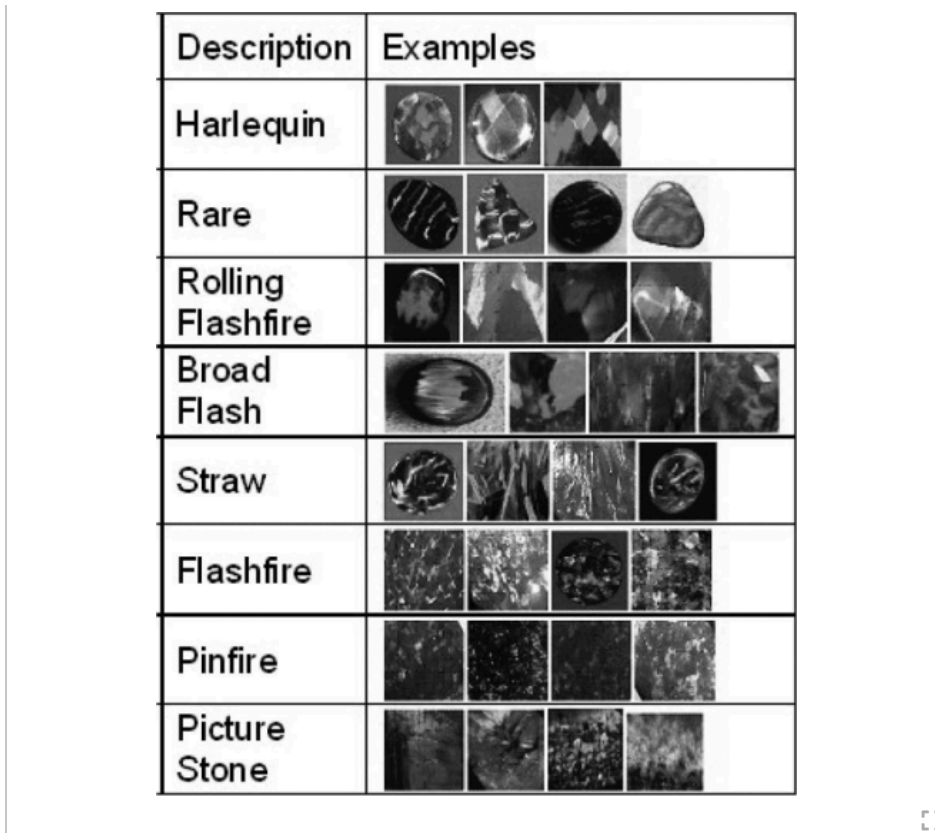
The automated grading model is specific to an opal's class. For each opal class, a separate SVR model is used. After the classification, the measured opal features are employed as the input to the

SVR model for calculating the gem score of the opal. The gem score is then used to produce the opal grade, which is associated with the market value of the opal per carat [47], [48].

The grading takes into account the opal flash measurement as calculated using (5), body tone including brightness and saturation, pattern, percentage of color in face, and POC. Fig. 18 shows some sample opal patterns. Pattern adjustment depends on the type of the pattern, for example, harlequin, rolling flash, broad flash, pinfire, ribbon, floral, etc. The percentage of color in the face will exclude potch and anything that is not crystalline opal, such as sand and boulder. These features together with the mean of observed values and the gem score (i.e., the average score on a per carat basis from manual valuations), are used as the training dataset to train an SVR model.

| Description       | Examples   |
|-------------------|--|
| Harlequin         |    |
| Rare              |    |
| Rolling Flashfire |    |
| Broad Flash       |    |
| Straw             |    |
| Flashfire         |   |
| Pinfire           |  |
| Picture Stone     |  |





**Fig. 18.** Sample opal patterns.

The training and testing are conducted in two rounds. In the first round of training and testing, outliers are identified by checking the predicted gem score values against the max and min values from the manual valuation. If the predicted value for a training sample falls outside the max and min band, the training sample is deemed to be an outlier. The outliers need to be removed from the training dataset because leaving them in the training dataset will increase variation and bias the estimates in the SVR.

With the trained SVR model, an opal gem score can be produced based on these opal features. A grade can then be assigned to the opal based on the gem score and preconfigured gem score thresholds for individual opal grades. For example, after the opal with delivery number 1061-02 is scanned and analyzed, its feature dataset is produced: (1384, 2.84, 4.86, 1, 100, 43.05). These values correspond to the following measurements: flash, BN, SN, pattern adjustment, percentage opal in face, and POC. This dataset is then used as the input to the trained SVR model; the gem score of the opal, 526, is hence generated. Table IV shows some sample training datasets for the opal grading.

**TABLE IV** Sample Training Dataset for Black Opals

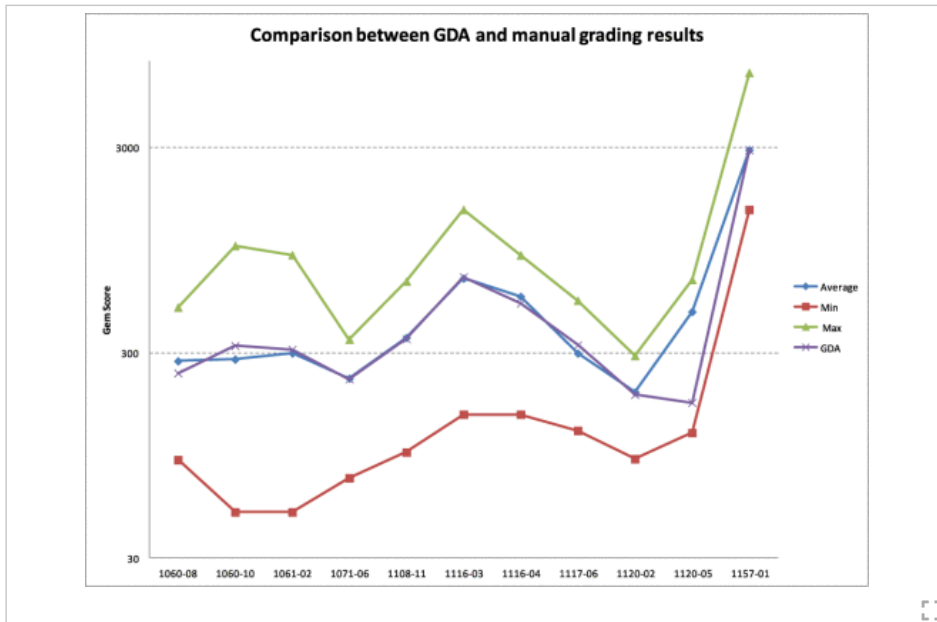
| Opal Delivery No | Flash Measurement | BN   | SN   | Pattern Adjustment | % Color in Face | Play of Color | Gem Score | Grade              |
|------------------|-------------------|------|------|--------------------|-----------------|---------------|-----------|--------------------|
| 1003-06          | 850               | 2.62 | 2.29 | 0.8                | 100             | 26.87         | 270       | Opallia™ A Black   |
| 1010-02          | 1429              | 2.2  | 1.32 | 0.8                | 100             | 51.58         | 824       | Opallia™ A+ Black  |
| 1014-02          | 3103              | 2.84 | 2.72 | 1.0                | 100             | 60.49         | 1207      | Opallia™ AA Black  |
| 1010-07          | 15769             | 2.8  | 5.54 | 1.0                | 100             | 74.28         | 1913      | Opallia™ AA+ Black |
| 1157-01          | 2286              | 2.36 | 1.25 | 1                  | 100             | 69.08         | 2906      | Opallia™ AAA Black |

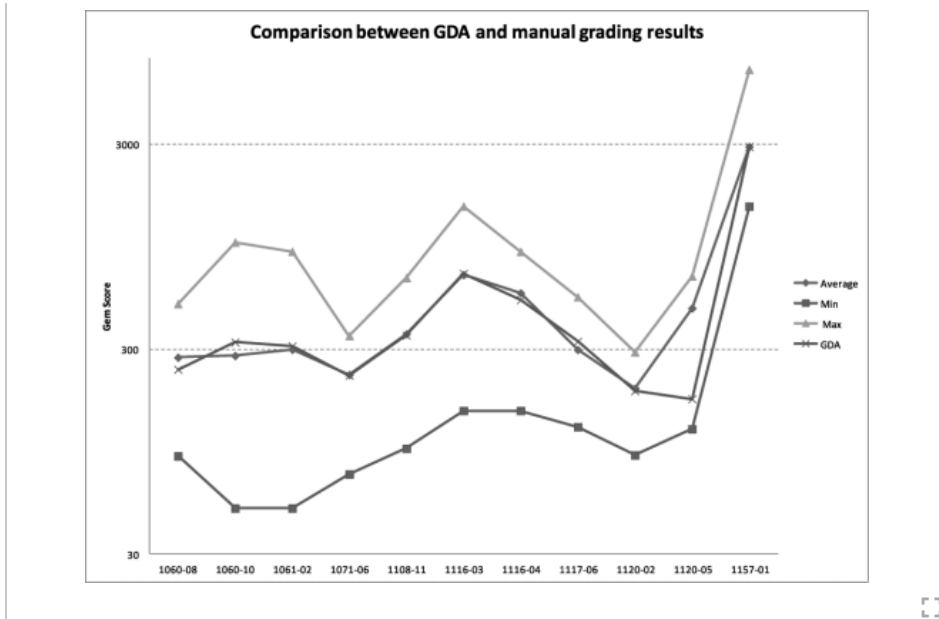
An opal can be graded into one of the grades listed in Table III, based on its gem score. In the table, dark means gray, and light means white. For example, in the previous example, the gem score of the opal is greater than 500 and less than 999 and the opal class is black, the opal is graded as Opallia A+ BLACK.

**TABLE III** Opal Grades and Corresponding Gem Scores

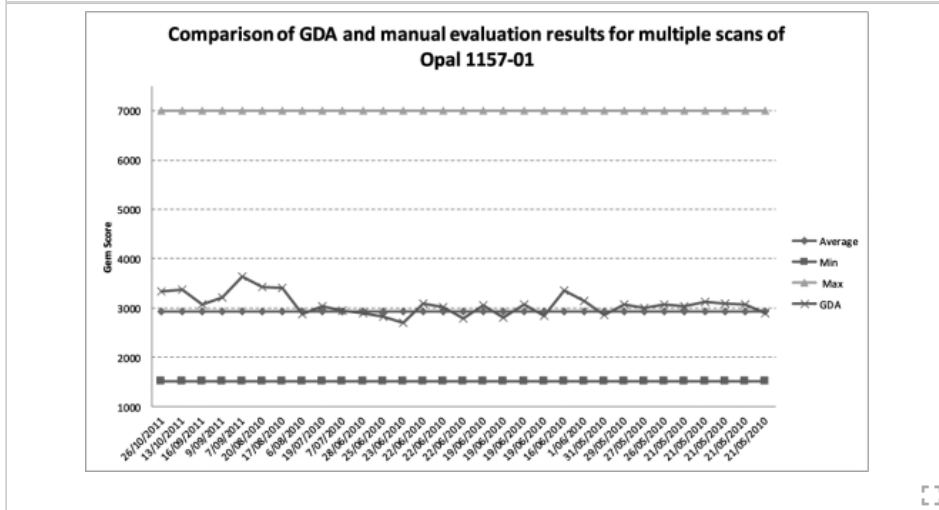
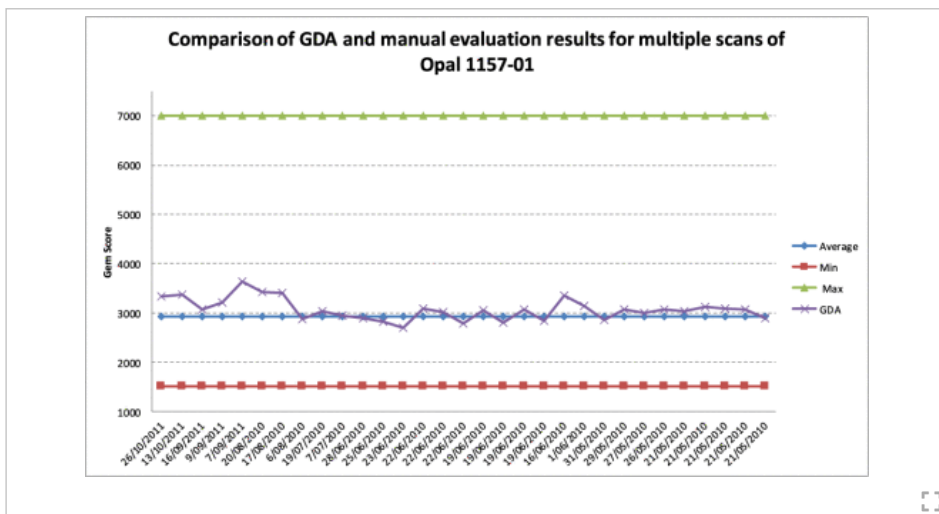
| Grade               | Gem Score                                       |
|---------------------|---|
| Opallia™ AAA+ BLACK | Gem Score $\geq 3000$                           |
| Opallia™ AAA BLACK  | Gem Score $\geq 2000$ and Gem Score $\leq 2999$ |
| Opallia™ AA+ BLACK  | Gem Score $\geq 1500$ and Gem Score $\leq 1999$ |
| Opallia™ AA BLACK   | Gem Score $\geq 1000$ and Gem Score $\leq 1499$ |
| Opallia™ A+ BLACK   | Gem Score $\geq 500$ and Gem Score $\leq 999$   |
| Opallia™ A BLACK    | Gem Score $\geq 0$ and Gem Score $\leq 499$     |
| Opallia™ BBB+ DARK  | Gem Score $\geq 3000$                           |
| Opallia™ BBB DARK   | Gem Score $\geq 2000$ and Gem Score $\leq 2999$ |
| Opallia™ BB+ DARK   | Gem Score $\geq 1500$ and Gem Score $\leq 1999$ |
| Opallia™ BB DARK    | Gem Score $\geq 1000$ and Gem Score $\leq 1499$ |
| Opallia™ B+DARK     | Gem Score $\geq 500$ and Gem Score $\leq 999$   |
| Opallia™ B DARK     | Gem Score $\geq 0$ and Gem Score $\leq 499$     |
| Opallia™ CCC+ LIGHT | Gem Score $\geq 3000$                           |
| Opallia™ CCC LIGHT  | Gem Score $\geq 2000$ and Gem Score $\leq 2999$ |
| Opallia™ CC+ LIGHT  | Gem Score $\geq 1500$ and Gem Score $\leq 1999$ |
| Opallia™ CC LIGHT   | Gem Score $\geq 1000$ and Gem Score $\leq 1499$ |
| Opallia™ C+ LIGHT   | Gem Score $\geq 500$ and Gem Score $\leq 999$   |
| Opallia™ C LIGHT    | Gem Score $\geq 0$ and Gem Score $\leq 499$     |

To verify the automated opal grading, we have conducted experiments using various classes of opals, including black, dark, white, crystal, and boulder. It should be noted, for different opal classes, we use different SVR models. The following discusses the results produced from the SVR model for black opals. In the experiment, we used 115 black opal samples as the training dataset. Some training samples are from the same opal but the opal was imaged at different times. This can be used to verify the consistency of the GDA performance when grading the same opal at different times. Figs. 19 and 20 demonstrate the comparison between the GDA and the manual valuation results.





**Fig. 19.** Comparison between the GDA and manual grading results for various opals.



**Fig. 20.** Comparison between the GDA and manual grading results for multiple scans of opal 1157-01.

The “max” and “min” shown in Figs. 19 and 20 correspond to the maximum and minimum gem scores obtained from the 60 experts’ manual valuations for individual opals used in the test. The “average” is the mean of the manual valuation results. The “GDA” is the gem score predicted by the SVR model.

The experimental results demonstrate that all predicted gem scores are within the max and min bands. The average prediction error is 16.64%.

To evaluate the performance of the GDA, we have also assessed the variability of the gem scores produced by the GDA. The coefficient of variation (CV) is employed to measure the variability. Table V shows the comparison of the CVs of the GDA produced gem scores and the gem scores obtained from the experts’ manual assessment for the opal with the delivery number 1157-01. The CV of the GDA produced gem scores is much smaller than that of the manual valuation results by the opal experts. This means that the GDA predicted gem scores are much less dispersed than the manual evaluation results, and the GDA predicted values are more consistent and closer to the actual values of opals than the manual results.

**TABLE V** Comparison of Coefficients of Variation of the GDA Produced Gem Scores and Experts’ Results

| Opal 1057-01 | Mean     | Standard Deviation | Coefficient of Variation (%) |
|--------------|----------|--------------------|------------------------------|
| Experts      | 2933.286 | 1623.93            | 55.36                        |
| GDA          | 3041.443 | 217.609            | 7.15                         |

#### 1) SVR Parameters:

Parameters used in the SVR are as follows.

- a) *SVR type*: Epsilon regression.
- b) Polynomial kernel,  $d(x, y) = (\text{gamma} \cdot (x \cdot y) + \text{Coef0})^{\text{degree}}$ , where  $x$  and  $y$  are two feature vectors in the input space, degree = 3, gamma = 0.143, and Coef0 = 0.
- c) The distance between feature vectors from the training set and the fitting hyper-plane must be less than 0.1.
- d) The penalty multiplier for outliers is 1.0. This is the cost of constraints violation.
- e) The termination criterion is either 100 000 for the maximum iteration or 0.000001 for the epsilon in the insensitive-loss function, whichever is reached first.

#### 2) Support Vector Regression Analysis:

The SVR model used for the opal grading produces a gem score for an opal when its features are used as input of the model. The gem score is composed of two parts, namely

$$\text{Gem Score} = \text{Value Predicted by the SVR Model} + \text{Residual.} \quad (15)$$

[View Source](#) 

The value predicted by the model is termed the “fitted value.” The residual is the random component of the gem score not explained by the systematic part of the model; it is the difference between the gem score for an opal produced from the SVR model and the mean of the manual valuation of the opal. Thus, the residual represents the portion of the validation data not explained by the model.

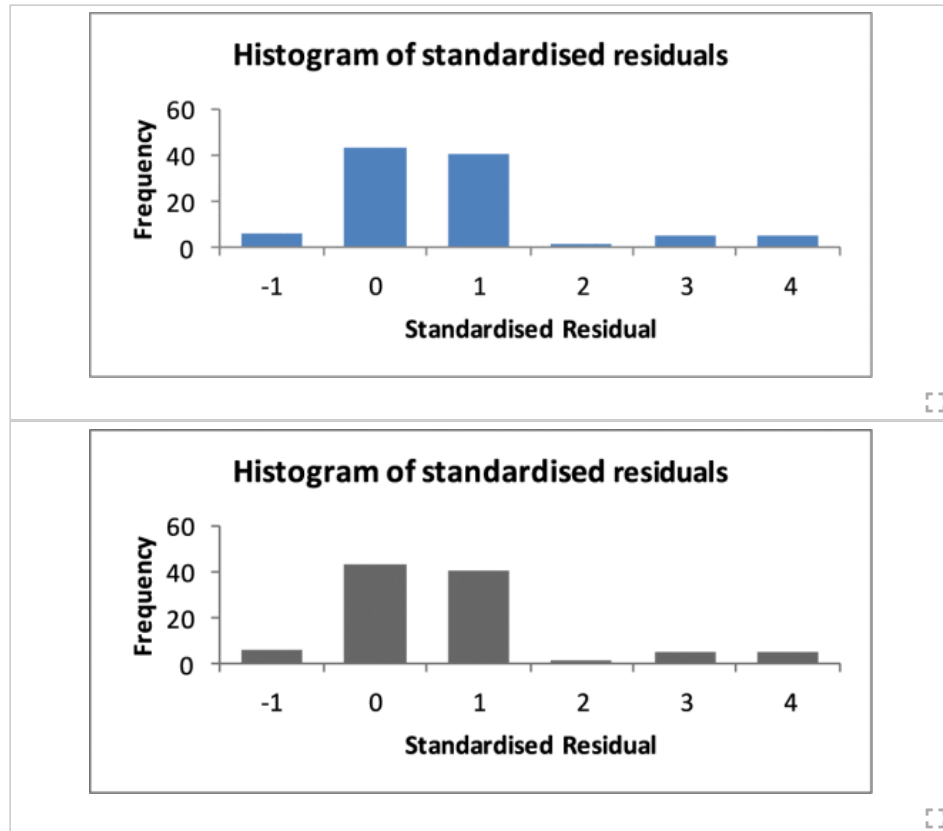
In the experiment, the histogram of standardized residuals can be plotted as shown in Fig. 21. Since the residual is in units of gem score, it is difficult to define what is a “large” residual. Therefore, the



standardized residual is used

$$\text{Residual} = \frac{\text{Residual}}{\text{Standard Error of the Residual}} \quad (16)$$

[View Source](#)



**Fig. 21.**  
Histogram of standardized residuals.

The histogram illustrates that the standardized residuals of most of opals are close to 0 or 1. This corresponds to the prediction results shown in Figs. 19 and 20.

## SECTION VI. Conclusion

In this paper, we have presented a machine vision system for automated opal grading. The system is composed of an automated image capture mechanism, software for the image analysis of opals, and the SVMs for automated opal classification and grading. The experimental results show that the opals in the training set could be classified with over 90% correct classification rate and the gem score can be automatically predicted using SVR. The average prediction error for the gem score is 16.64% and all predicted gem scores are within the max and min bands of the manual valuation, and are also in the vicinity of the averaged values of the manual valuation. The results indicate that the SVMs can be used in automated opal classification and grading if proper training samples are provided.

The limited number of opals available for the experiments may compromise the results. More opal samples from various classes and various grades within each class would help improve experimental results, for both classification and grading.

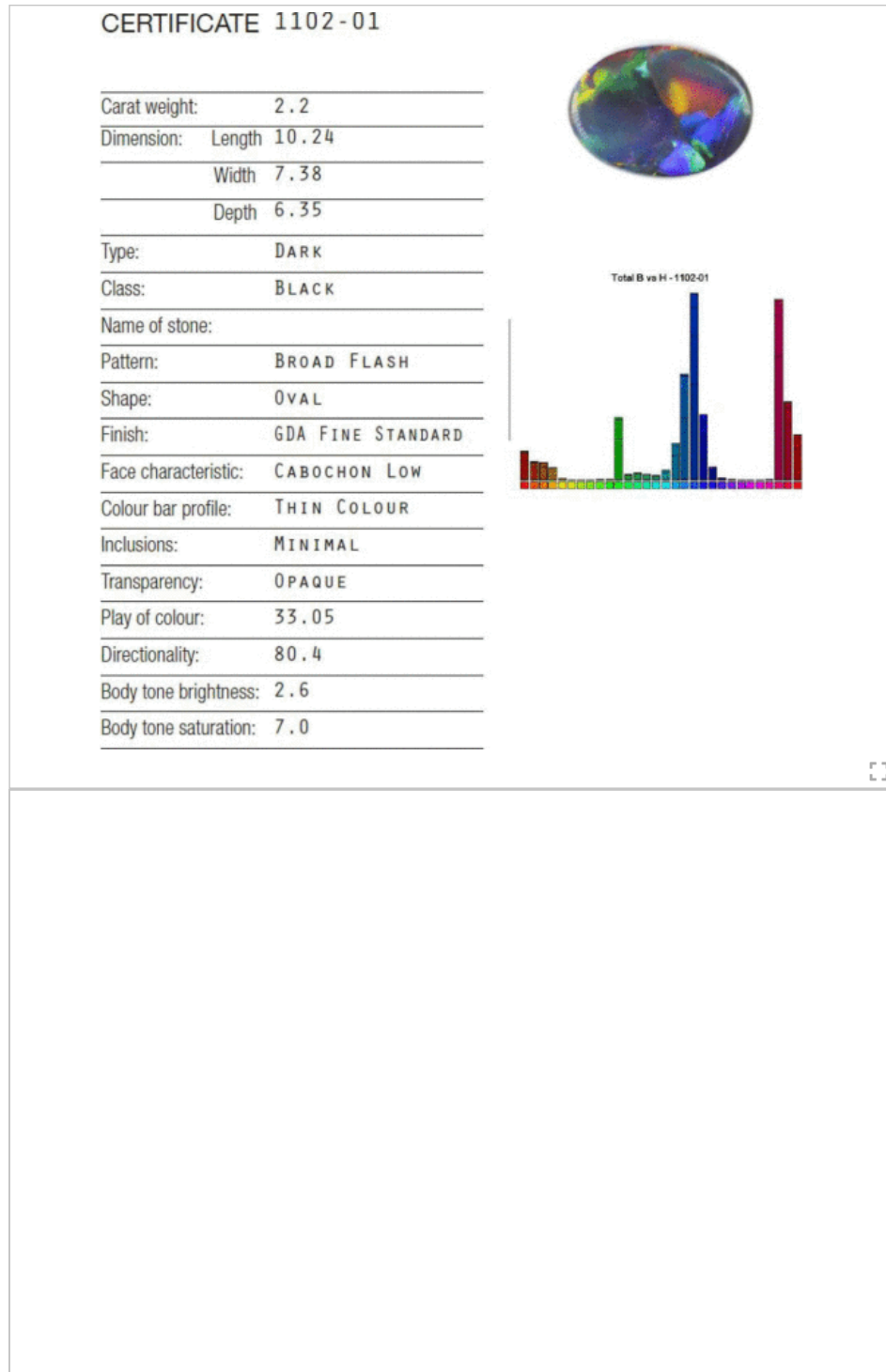
Opal is the hardest gemstone to evaluate because of its complex reflectance properties. The GDA has potential to be extended to grade other gem stones.

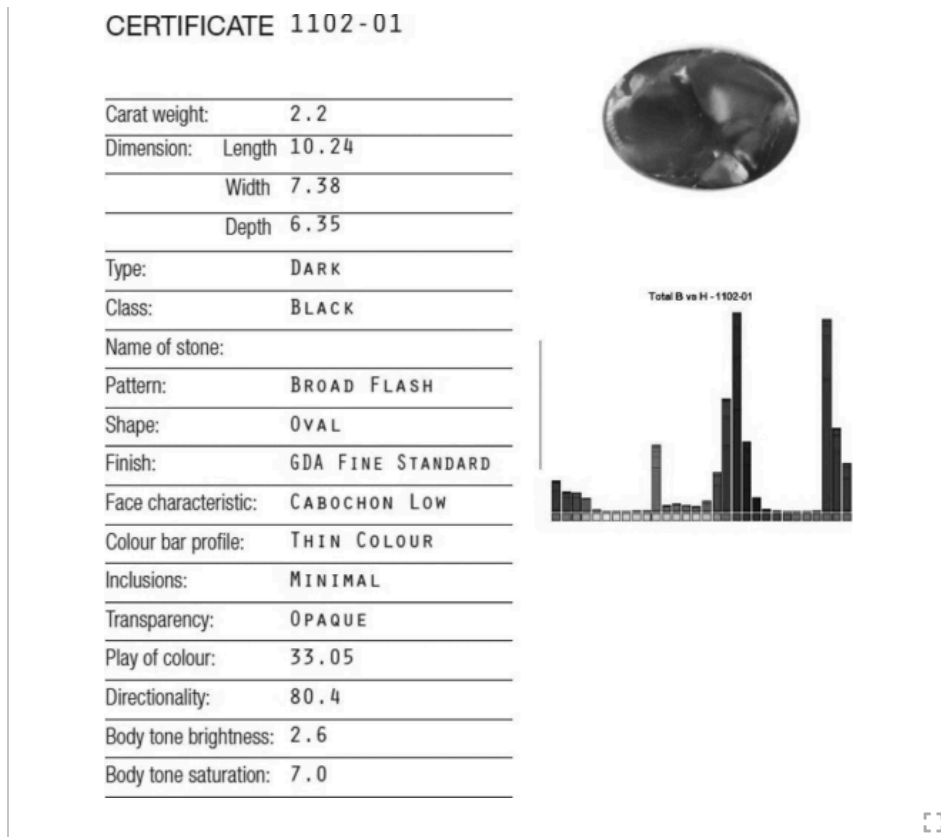
## ACKNOWLEDGMENT

The authors would like to thank the management of Opal Producers Australia Ltd. for granting us permission to use the images and results in this paper. They would also like to thank the insightful comments of the reviewers, and the valuable suggestions of the editors.

## Appendix

Fig. 22 shows sample GDA certificate.





**Fig. 22.** Sample opal certificate produced by the GDA.

- Authors ▼
- Figures ▼
- References ▼
- Citations ▼
- Keywords ▼
- Metrics ▼

**More Like This**

Integrated literate programming for structured light camera calibration

2012 Joint Conference New Trends In Audio & Video And Signal Processing: Algorithms, Architectures, Arrangements And Applications (NTAV/SPA)

Published: 2012

Auto-calibration of emission spectra of light sources captured using camera spectrometer

2015 International Conference on Smart Sensors and Systems (IC-SSS)

Published: 2015

Show More

**IEEE Personal Account**

CHANGE  
USERNAME/PASSWORD

**Purchase Details**

PAYMENT OPTIONS  
VIEW PURCHASED  
DOCUMENTS

**Profile Information**

COMMUNICATIONS  
PREFERENCES  
PROFESSION AND  
EDUCATION  
TECHNICAL INTERESTS

**Need Help?**

US & CANADA: +1 800  
678 4333  
WORLDWIDE: +1 732  
981 0060  
CONTACT & SUPPORT

**Follow**



[About IEEE Xplore](#) | [Contact Us](#) | [Help](#) | [Accessibility](#) | [Terms of Use](#) | [Nondiscrimination Policy](#) | [IEEE Ethics Reporting](#) | [Sitemap](#) | [IEEE Privacy Policy](#)

A not-for-profit organization, IEEE is the world's largest technical professional organization dedicated to advancing technology for the benefit of humanity.

© Copyright 2024 IEEE - All rights reserved, including rights for text and data mining and training of artificial intelligence and similar technologies.

**IEEE Account**

» [Change Username/Password](#)

» [Update Address](#)

**Purchase Details**

» [Payment Options](#)

» [Order History](#)

» [View Purchased Documents](#)

**Profile Information**

» [Communications Preferences](#)

» [Profession and Education](#)

» [Technical Interests](#)

**Need Help?**

» **US & Canada:** +1 800 678 4333

» **Worldwide:** +1 732 981 0060

» [Contact & Support](#)

[About IEEE Xplore](#) | [Contact Us](#) | [Help](#) | [Accessibility](#) | [Terms of Use](#) | [Nondiscrimination Policy](#) | [Sitemap](#) | [Privacy & Opting Out of Cookies](#)

A not-for-profit organization, IEEE is the world's largest technical professional organization dedicated to advancing technology for the benefit of humanity.

© Copyright 2024 IEEE - All rights reserved. Use of this web site signifies your agreement to the terms and conditions.